Absorption spectroscopy of neighbouring Z plasmas in the X and XUV ranges at LULI 2000

G. Loisel, F. Thais (PI), T. Blenski, M. Poirier, S. Turck-Chièze, J-E Ducret*, D. Gilles
CEA/DSM - *CELIA - University of Bordeaux, France

S. Bastiani-Ceccotti (co-PI) and on-site operating teams
École Polytechnique / LULI, France

P. Arnault, T. Caillaud, J. Fariaut, F. Gilleron, J.-C. Pain, C. Reverdin, V. Silvert, B. Villette
CEA/DIF, France

W. Fölsner
Max-Planck-Institut für Quantenoptik, Germany

Contributors

F. Delahaye, C. Zeippen OBSPM, France
C. Blancard, G. Faussurier, P. Cossé CEA/DIF, France
J. Guzik, N. Magee, D. Kilcrease LANL, USA
J. Harris AWE, UK
M. Busquet LPGP, France

4th EMMI workshop on Plasma Physics - May 2-4, 2011, Darmstadt

Objectives

Provide knowledge of physical fundamental microscopic data necessary for the study of stellar interiors and the simulation of ICF

- Produce plasmas in LTE conditions at relatively high temperature (15-40 eV) for densities of a few 10 mg/cm^3
- Measure LTE plasmas spectral opacities in soft X-ray (700-1600 eV) and XUV (50-200 eV) domains
- Use of particular elements resonant absorption transitions in L and M shells
- Study atomic physical effects of multicharged ions in a plasma by varying the atomic number of the pure element plasma
- Confront experimental results with different theoretical approaches (detailed or statistical)

Opacity measurement principle

using laser and cavity «tools»

(1) Sample heating → laser beam 100-200 J - 0.5 ns - foc ~400 µm

(2) Radiography → laser beam 1-30 J - 10-30 ps - foc ~20 µm - delay ~0.5-3.5 ns

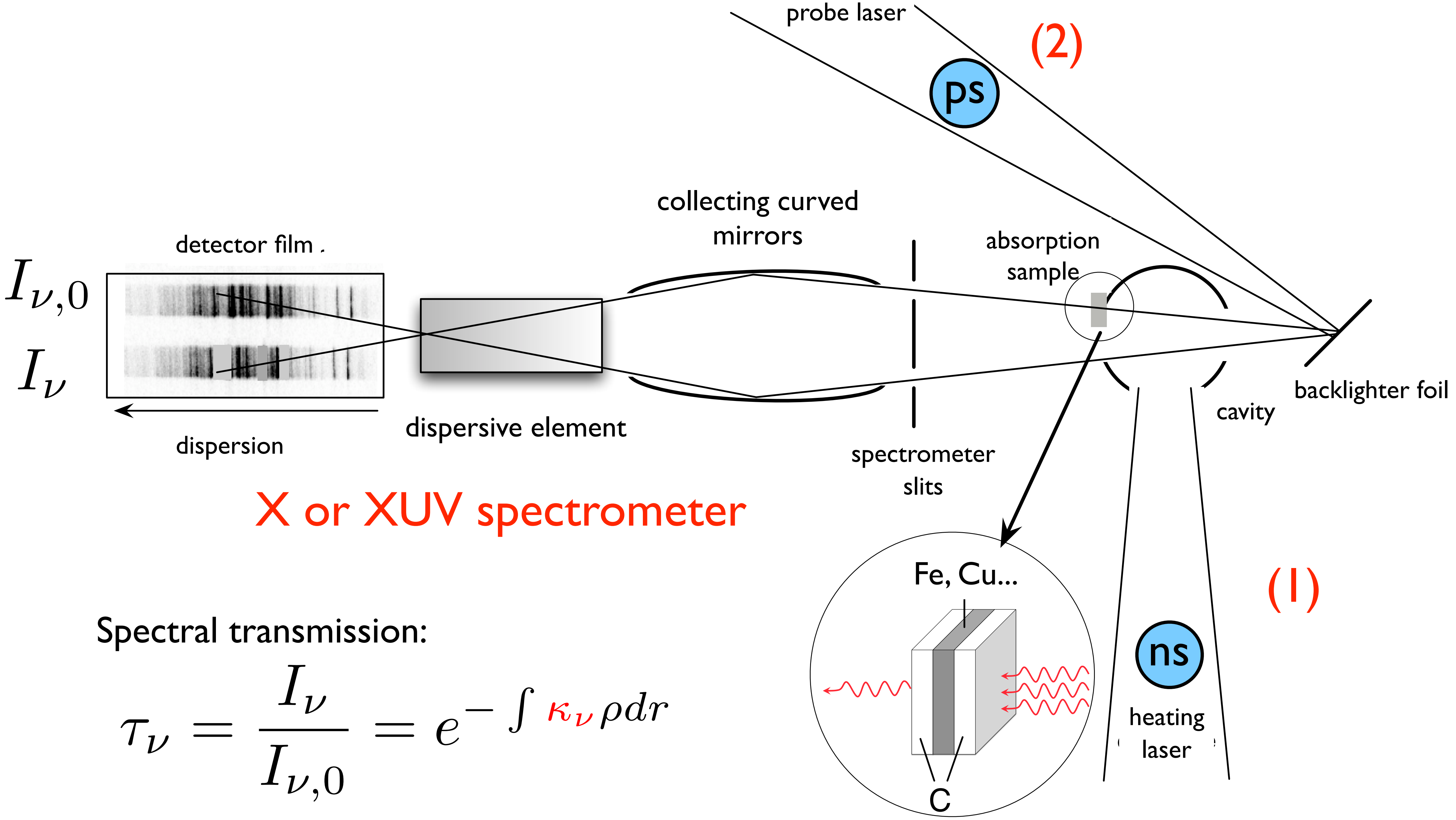

X or XUV spectrometer

Spectral transmission:

$$\tau_\nu = \frac{I_\nu}{I_{\nu,0}} = e^{-\int \kappa_\nu \rho dr}$$

X-ray opacity measurements

X-ray opacity measurements

Element selection

Exp 1 - 2008 Z = 26, 28, 29 & 32

Exp 2 - 2009 Z = 9, 56, 62, 64 & 67

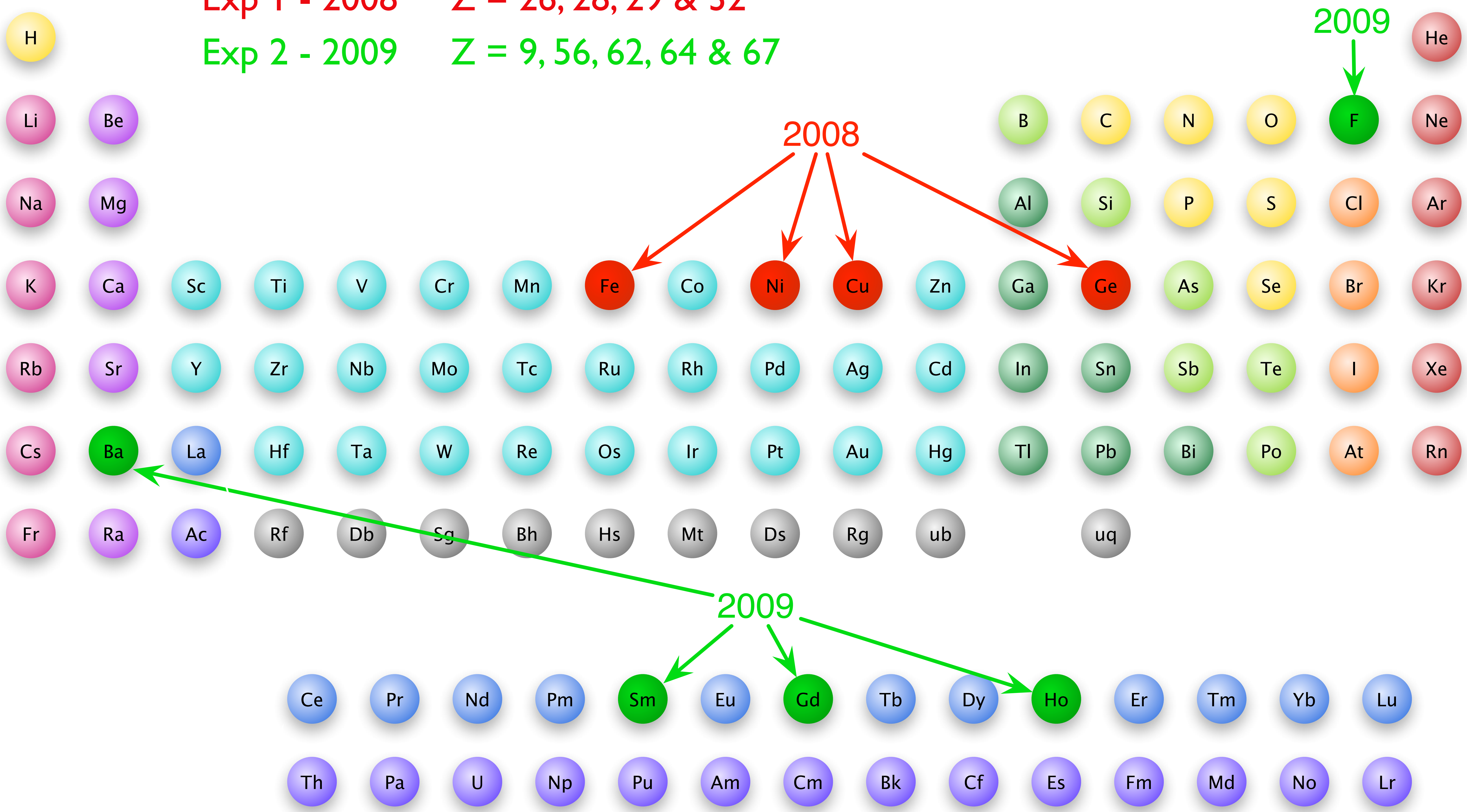

X-ray opacity measurements

Theoretical predictions

➡ Absorbing transitions 2p-3d of ions showing a spin-orbit-splitting strongly dependent on the atomic number and plasma conditions

➡ Test of the competition between spin-orbit-splitting and statistical broadening

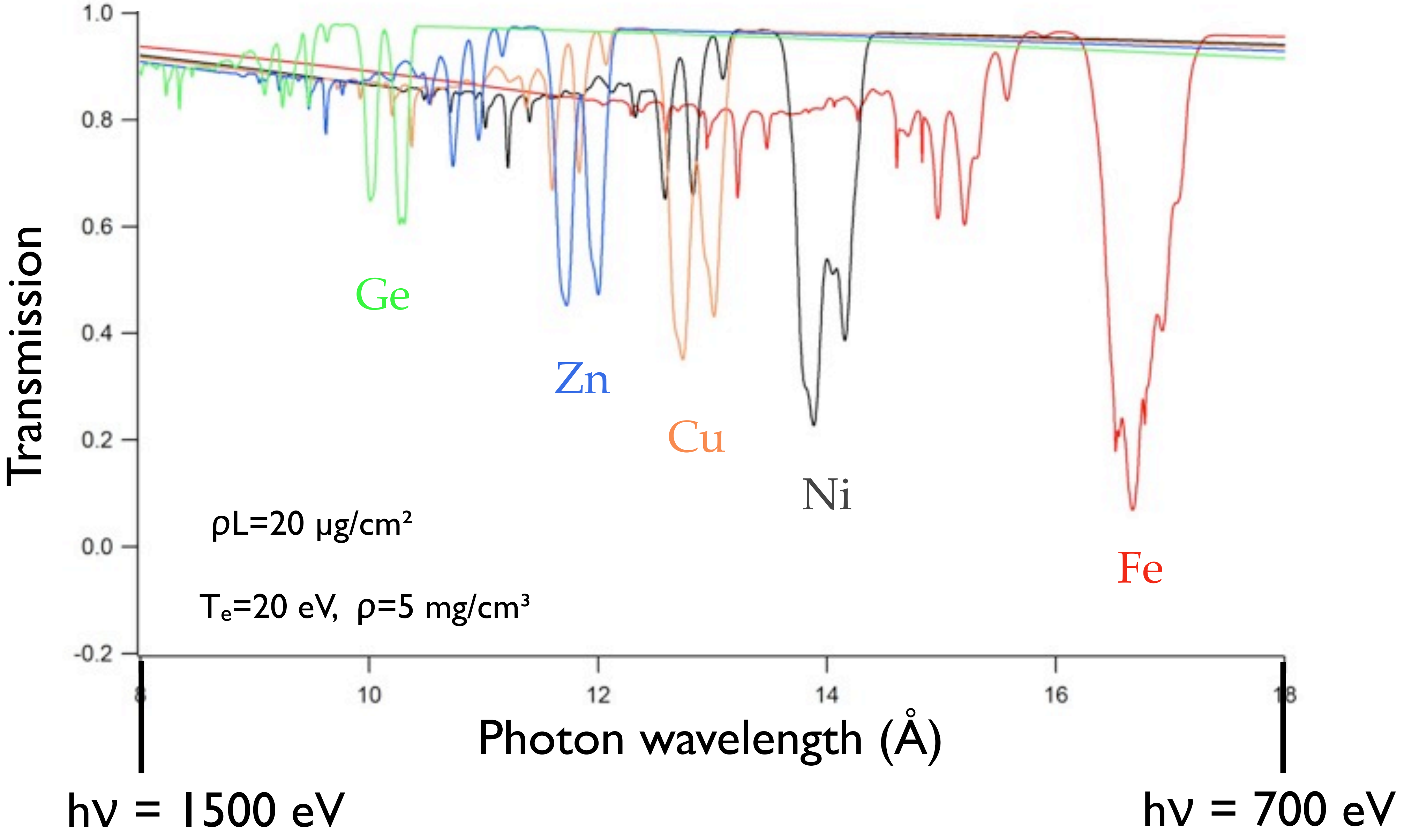

Calculations SCO : T. Blenski et al. 2000

X-ray opacity measurements

Experimental setup

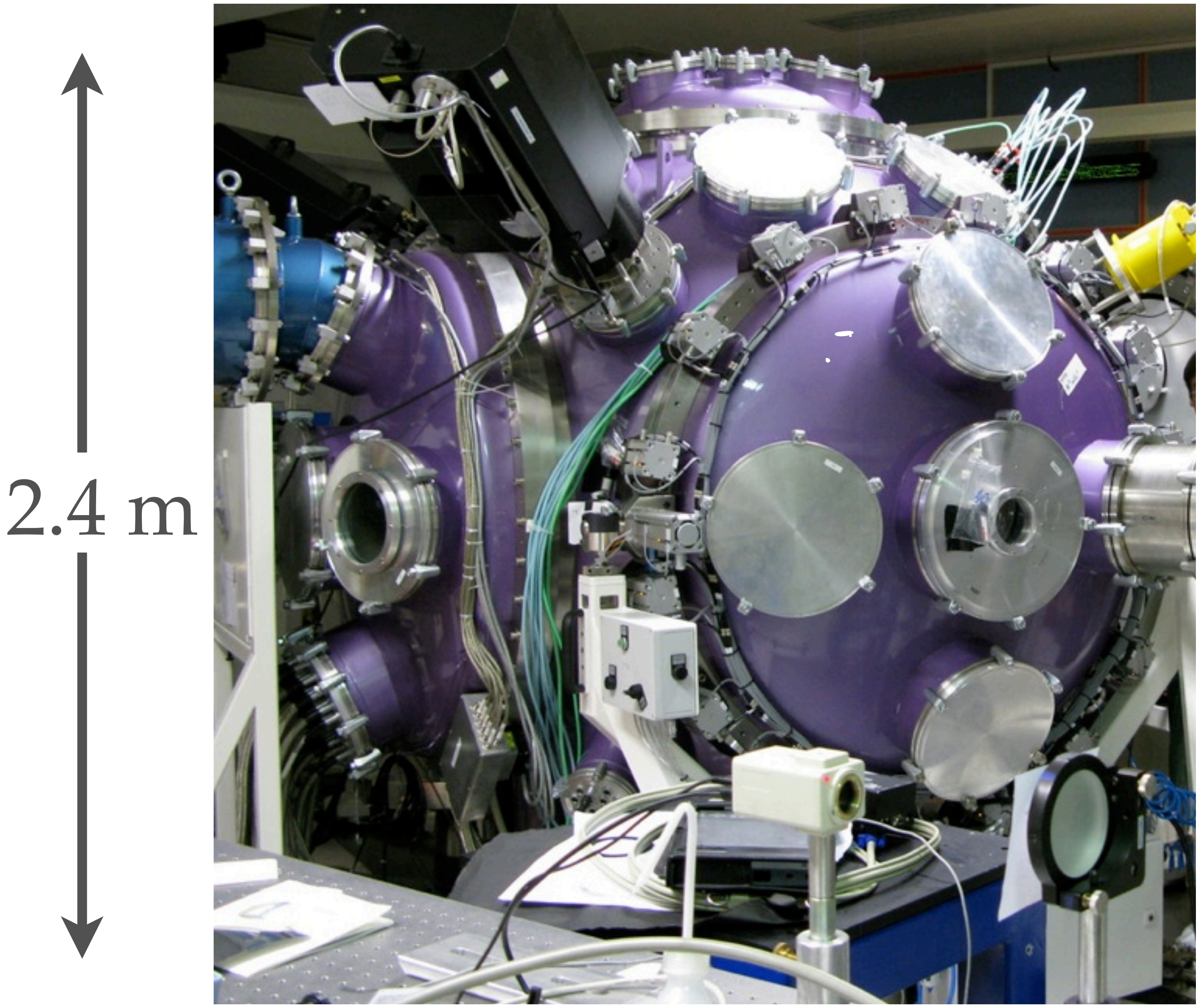

«Milka» experimental room

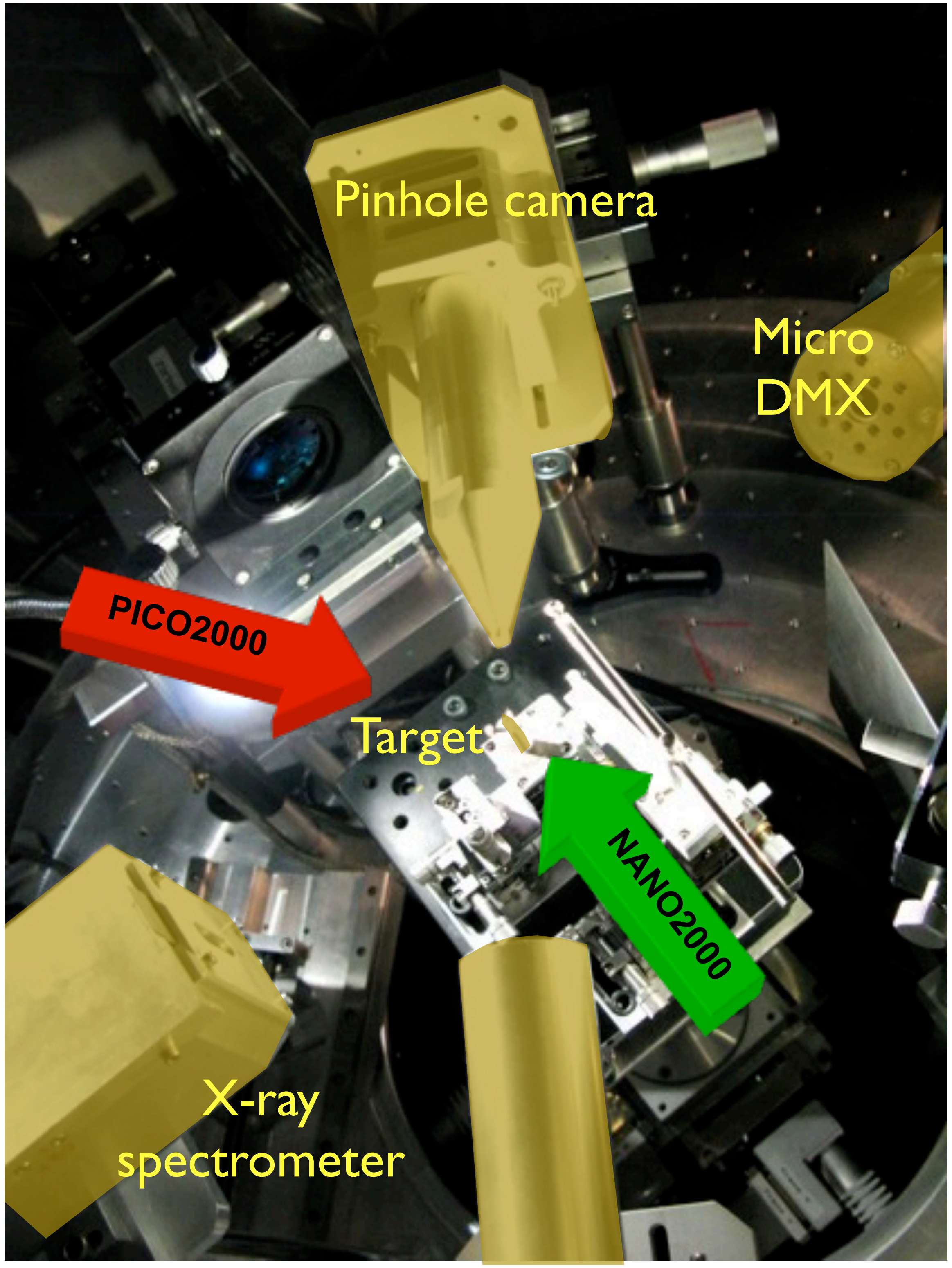

X-ray opacity measurements

Targets

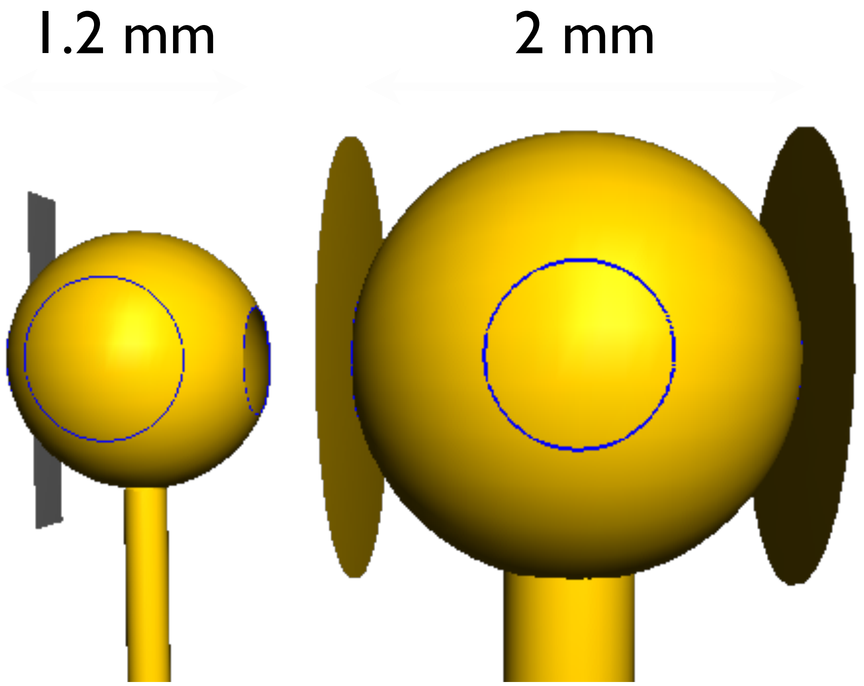

2008

2009
“Mickey Mouse”
cavity

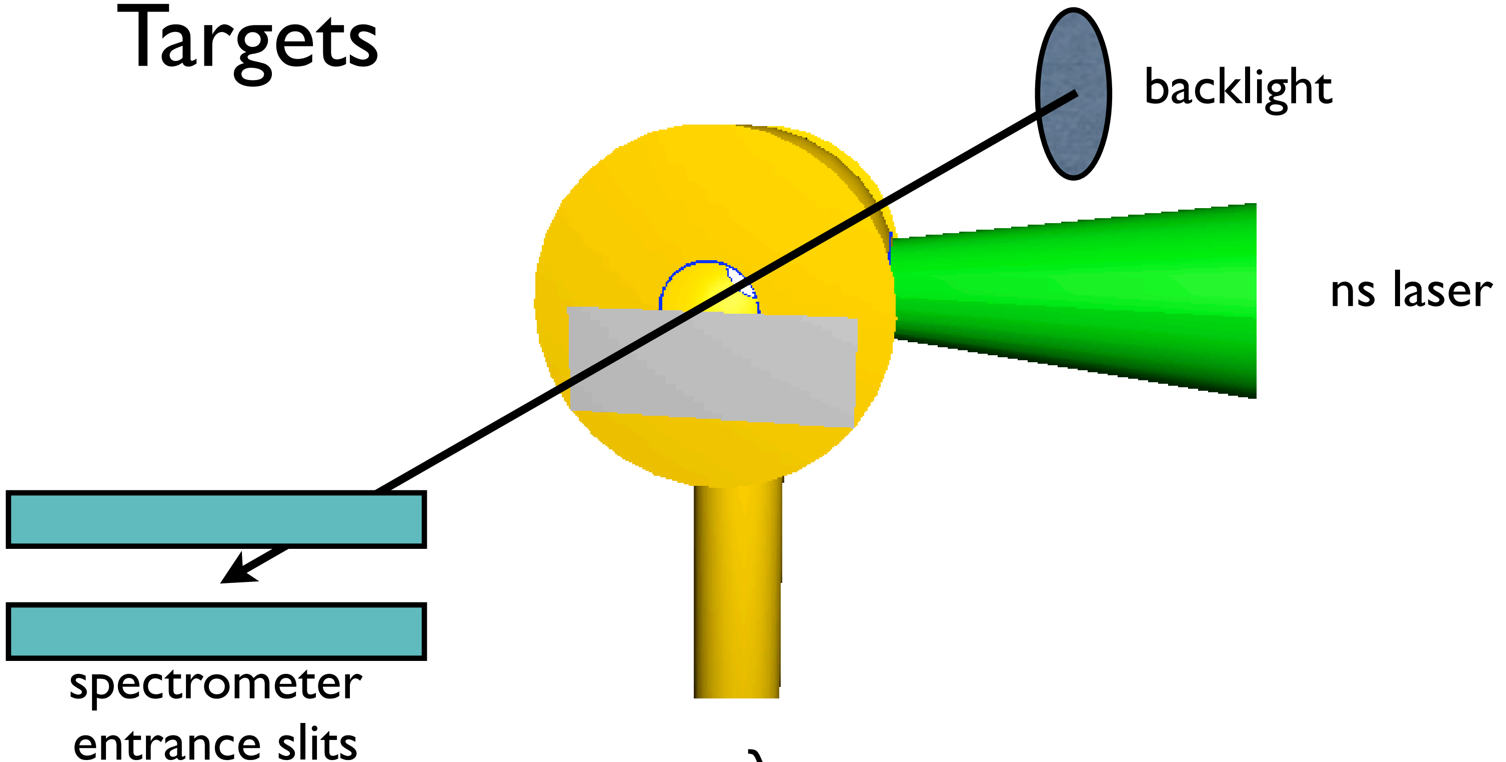

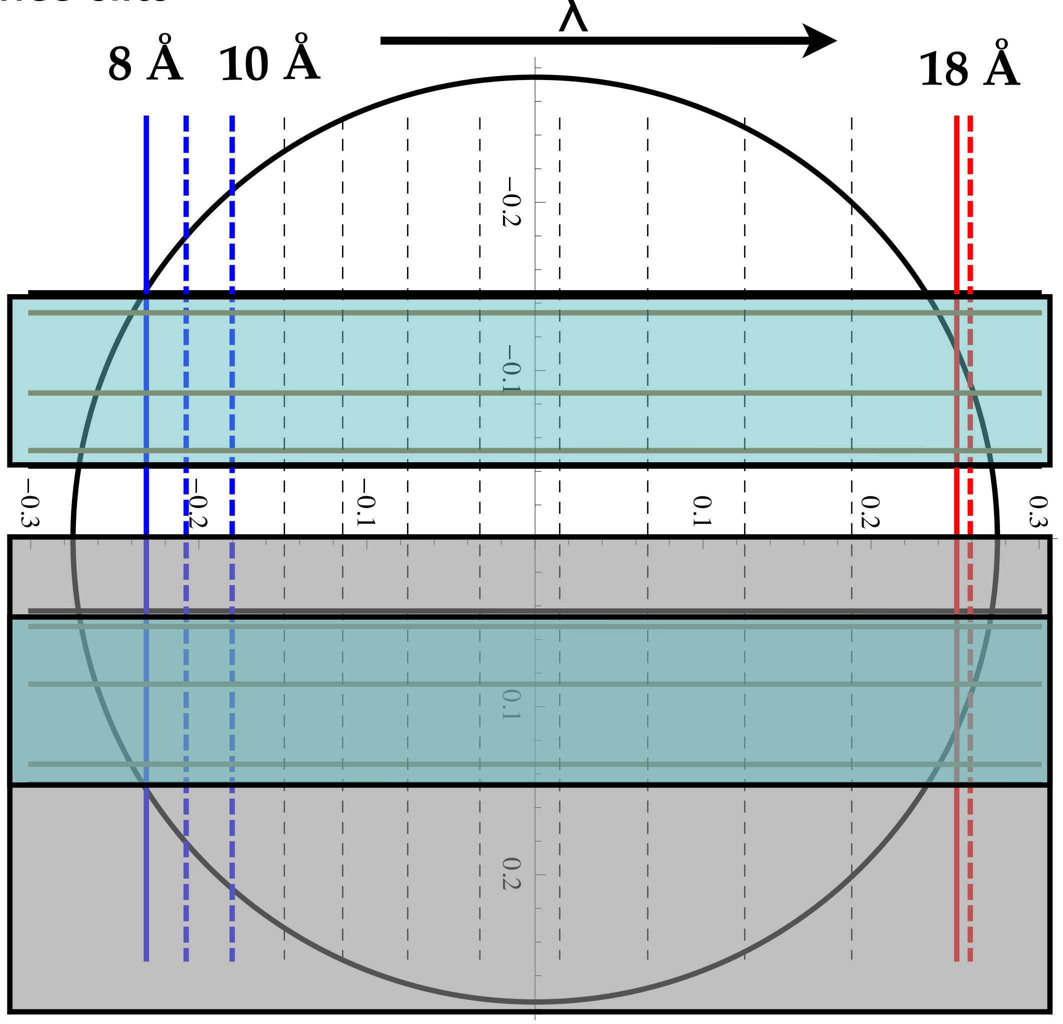

line of sight selection

Projection of selecting slits and spectral range on cavity diagnostic hole

X-ray opacity measurements

Targets

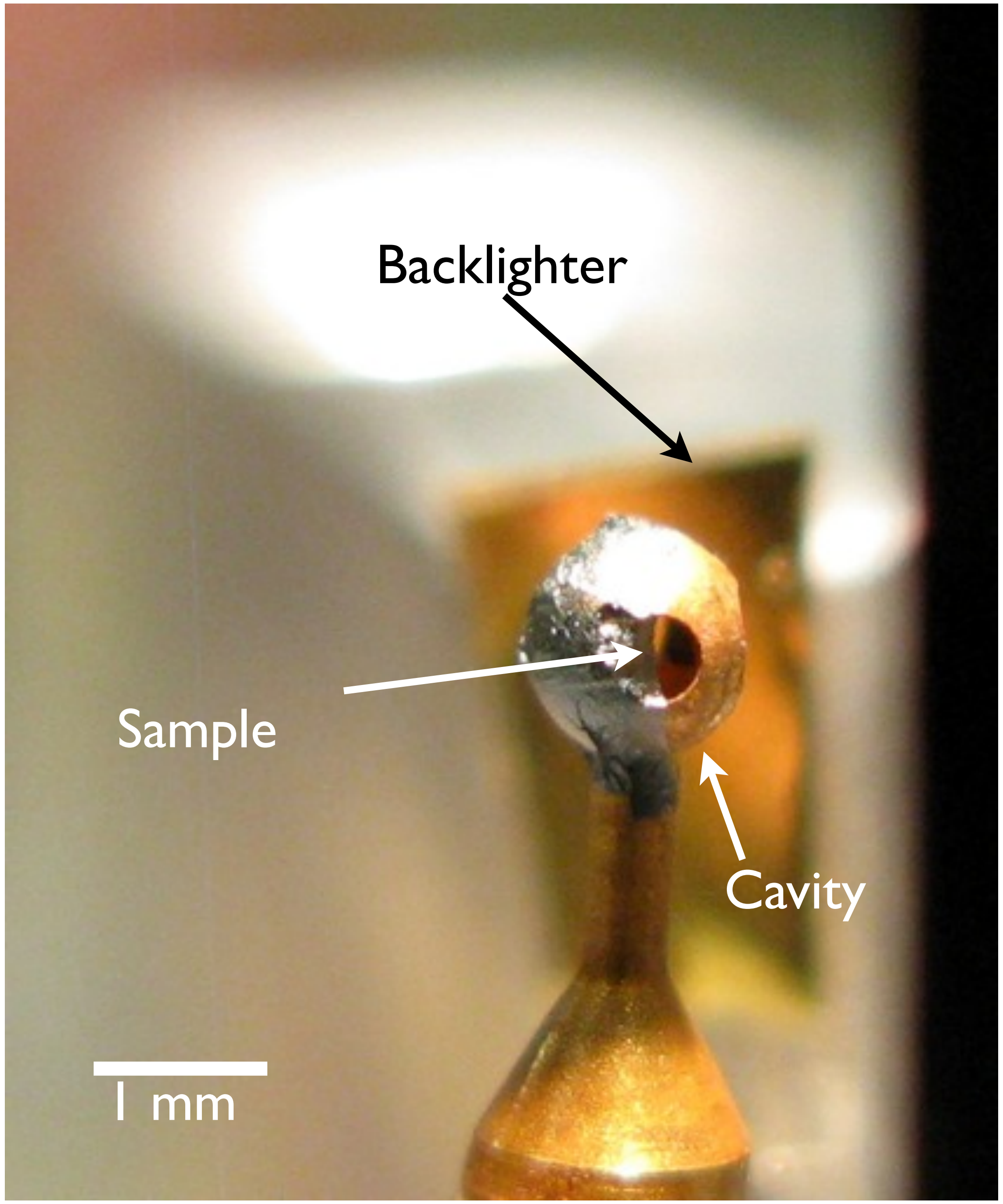

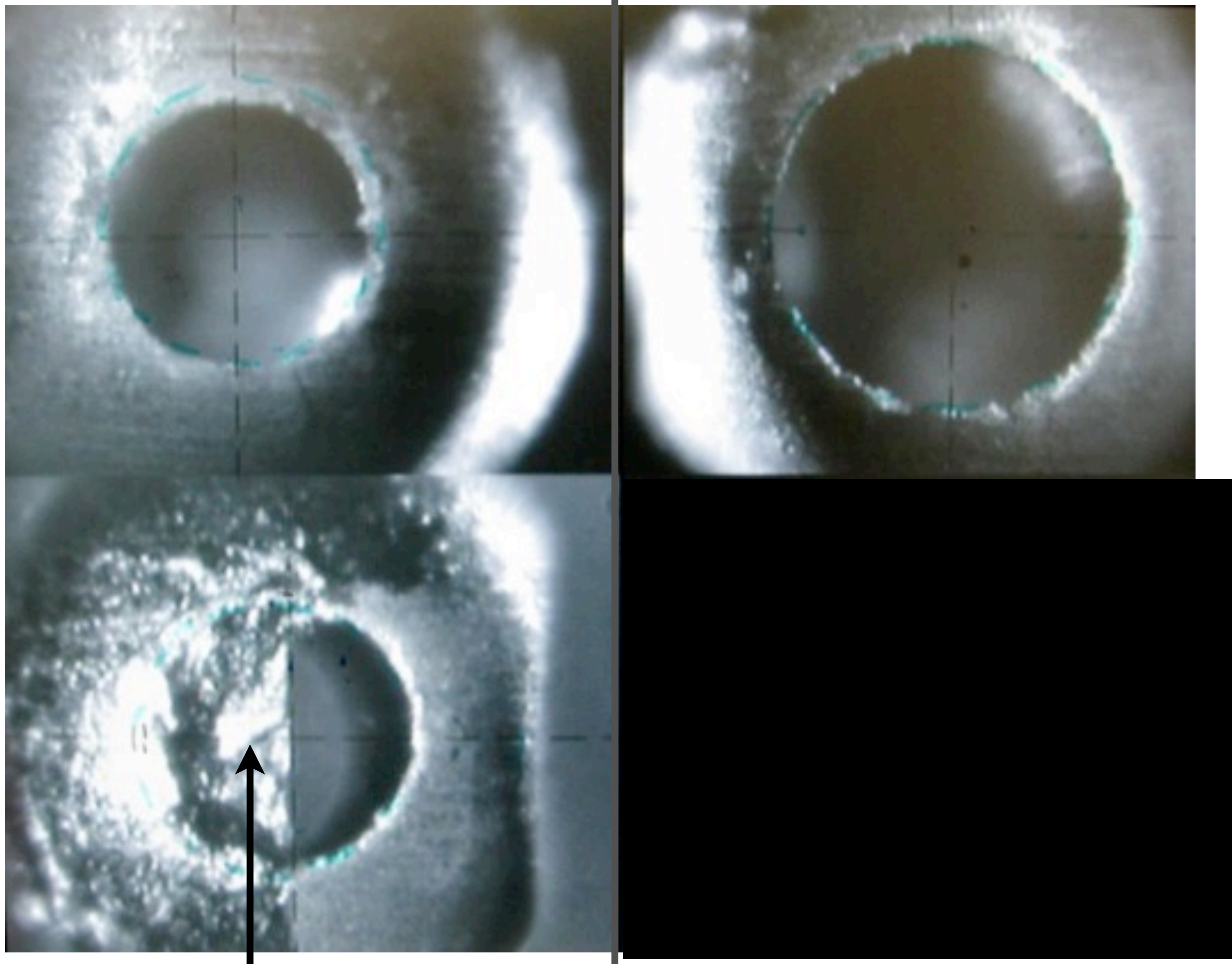
Diagnostic hole (Φ 500 µm)

Laser entrance hole (Φ 700 µm)

Sample thickness ~0.1 µm

X-ray opacity measurements

Diagnostics

X-ray spectrometer

- independent line of sights
- large spectral range 8 - 18 Å
- resolving power $<\lambda/\delta\lambda>\sim400$

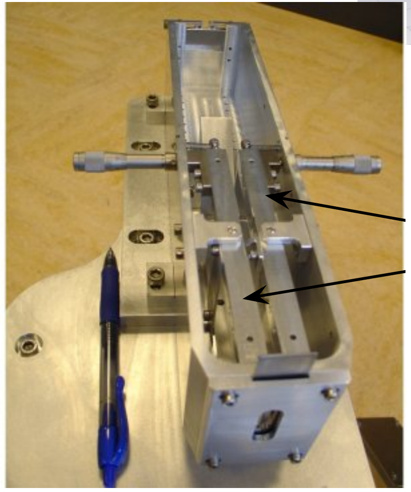

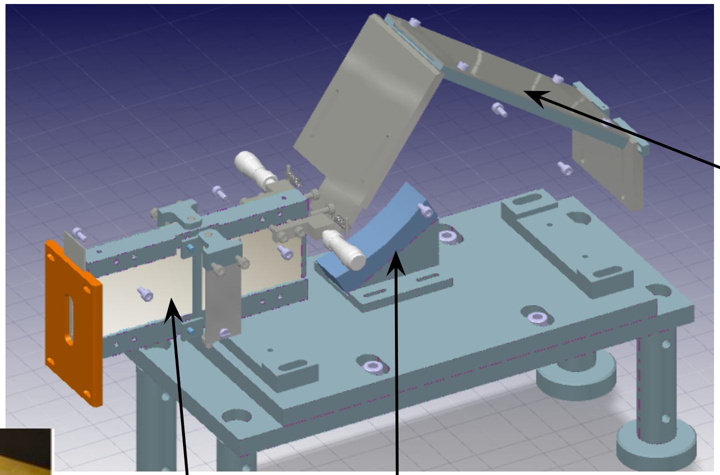

Detector : Imaging plates

TlAP cylindrical crystal

Concentrating spherical mirrors (grazing angle 1.5°, cut $h\nu>2$keV)

Reverdin, Thais, Loisel & Bougeard, RSI, 2010

Pinhole cameras

➡ image of emitting regions >1keV

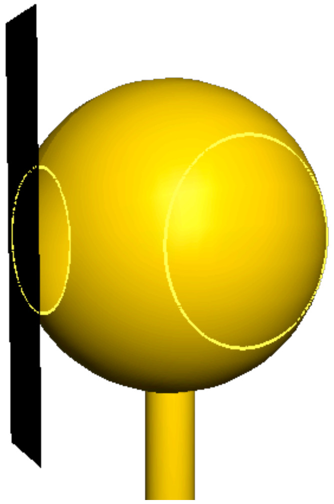

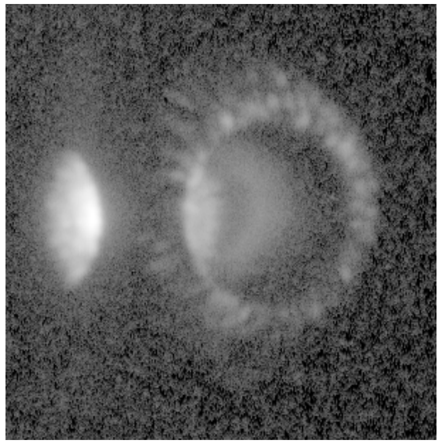

«micro-DMX» spectrometer

- absolute heating flux measurements
- time resolved
- 12 channels → broadband measurement

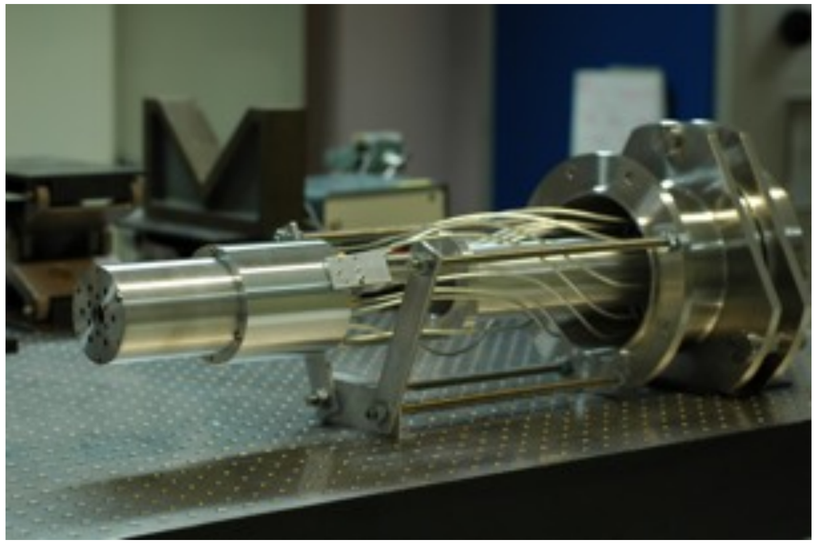

X-ray opacity measurements

Spectra extraction

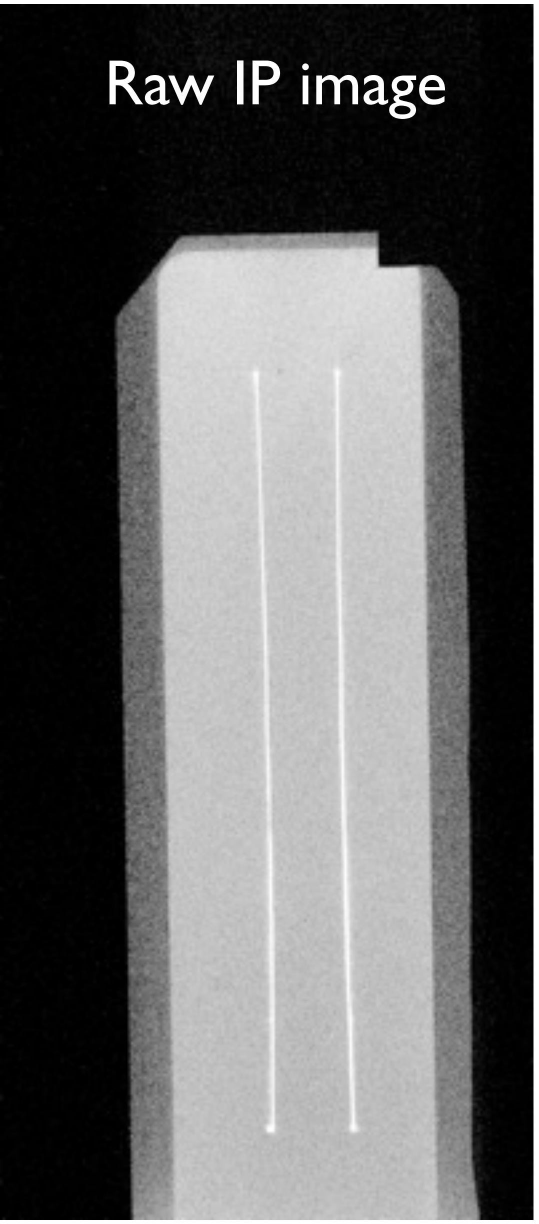

geometrical transforms

linearization

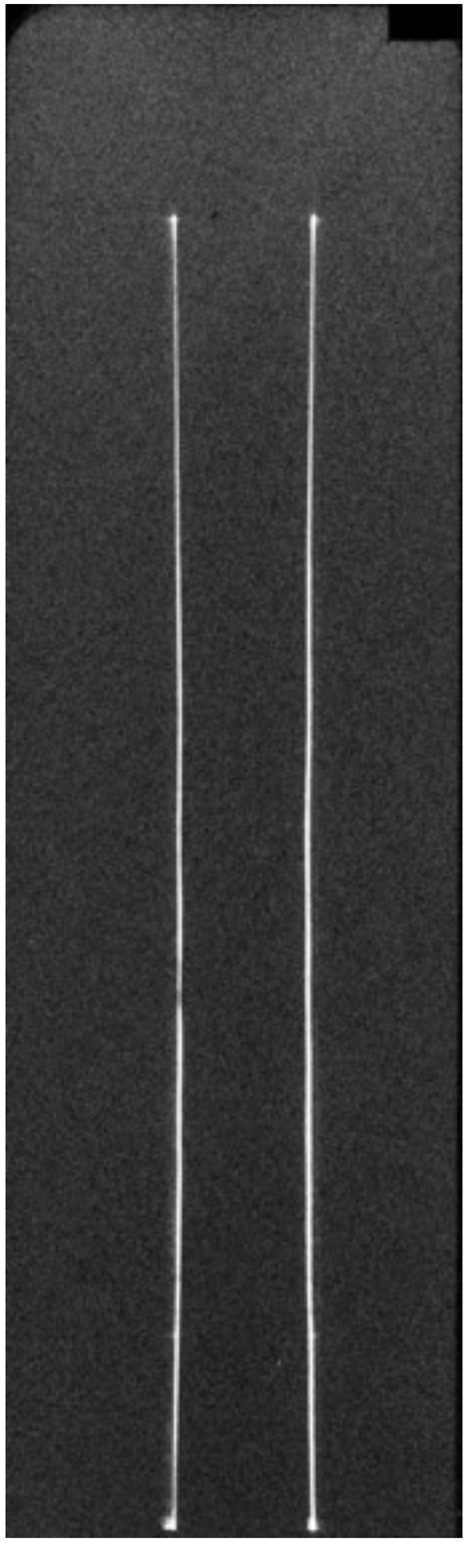

Gaussian &

wavelets filterings

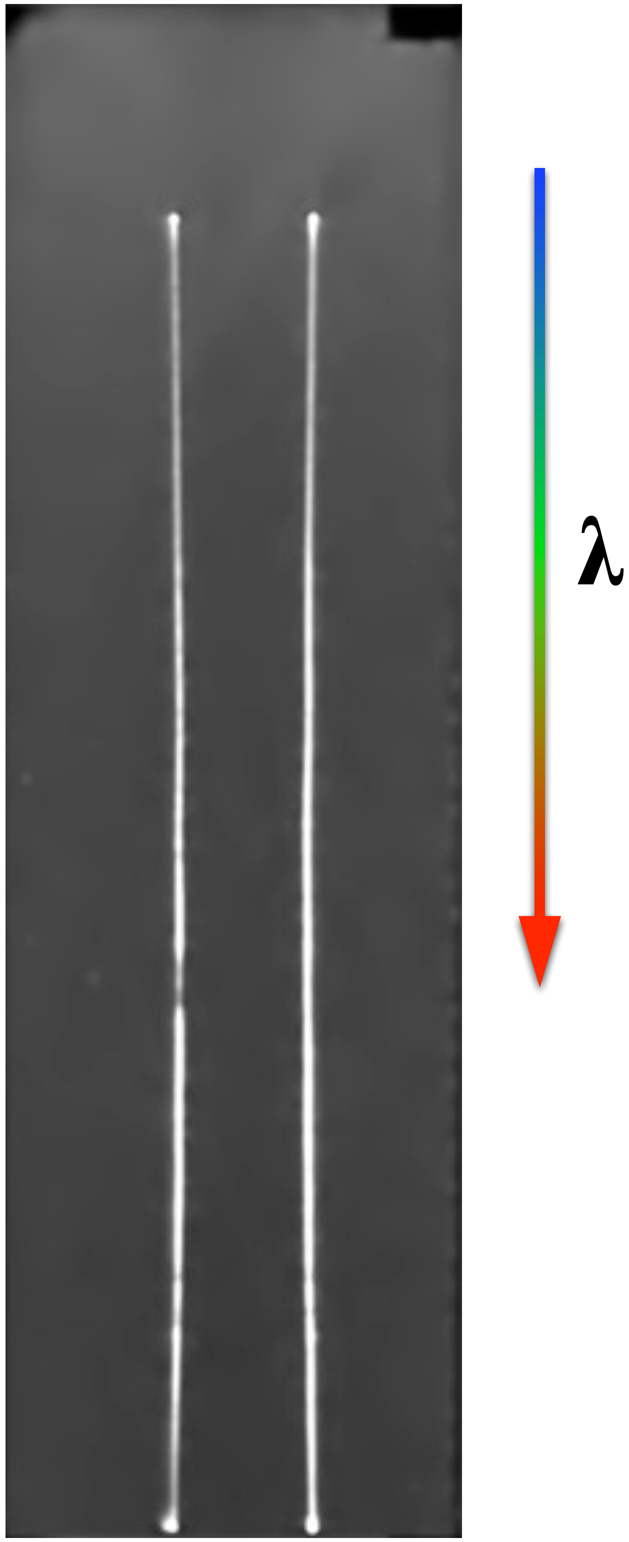

Spectral intensity

∝ transverse integral

X-ray opacity measurements

Spectra extraction

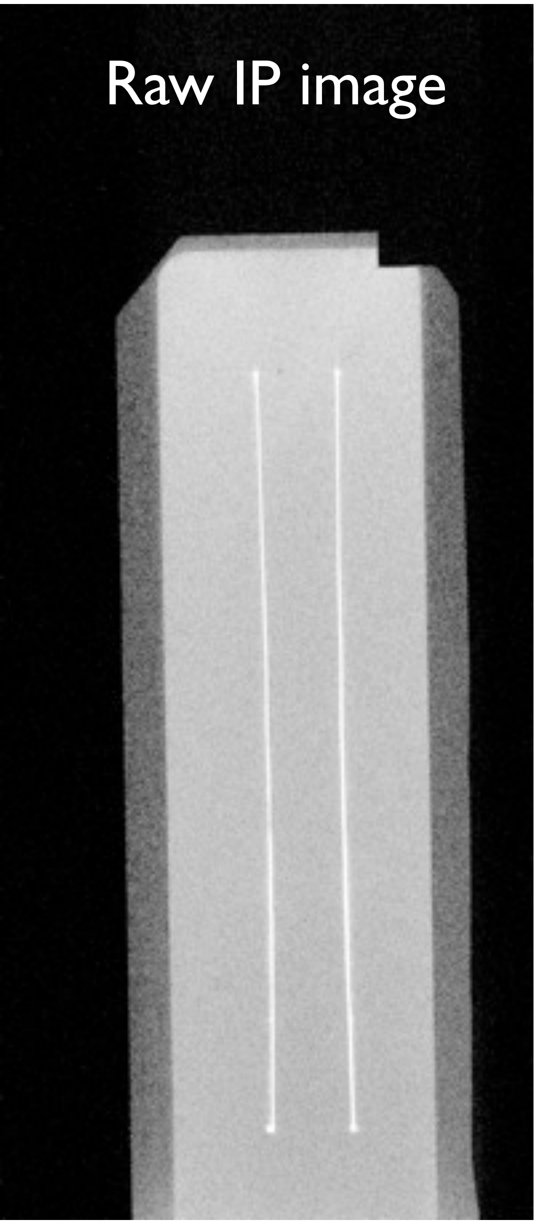

geometrical transforms

linearization

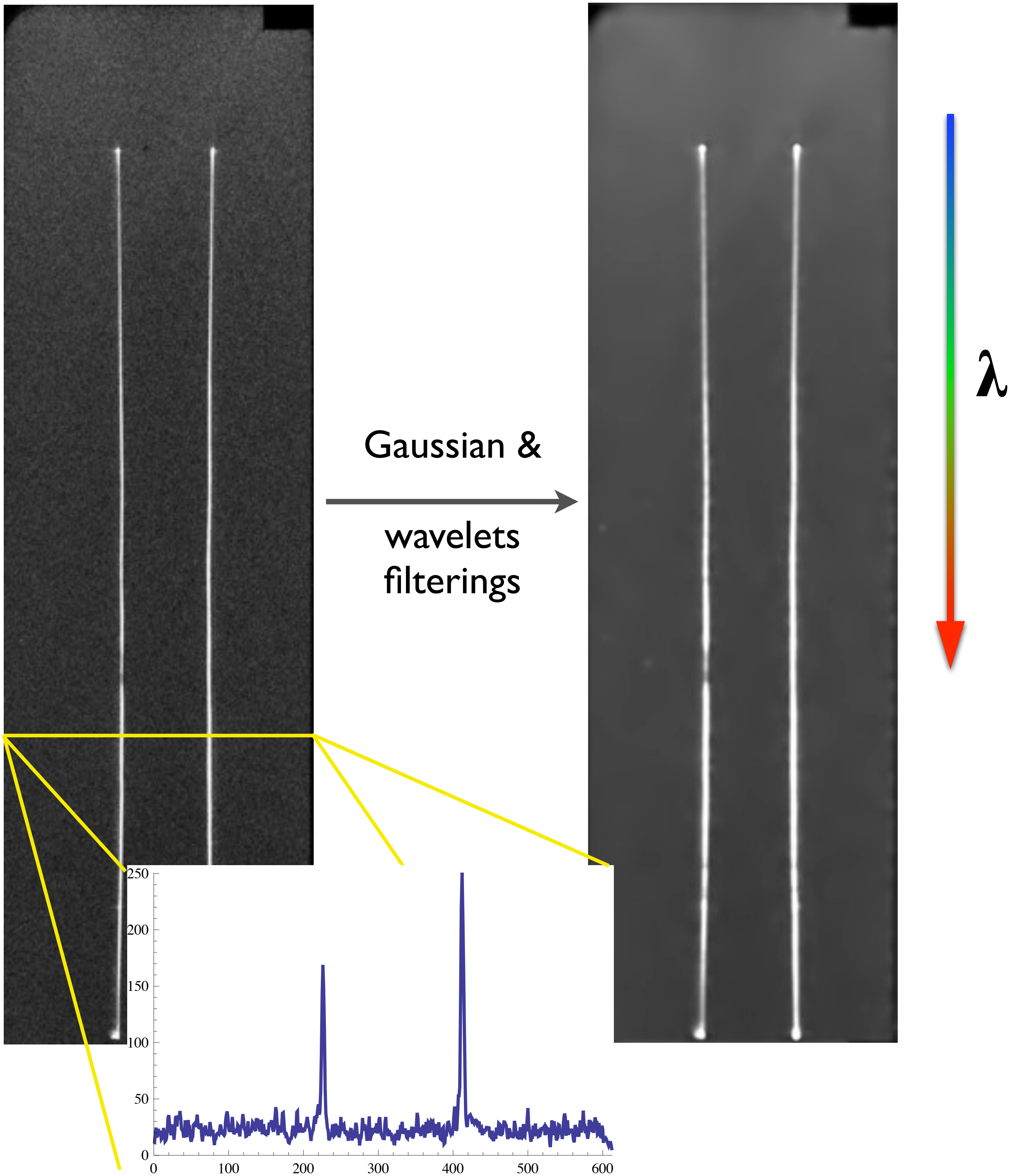

Gaussian &

wavelets filterings

Spectral intensity

∝ transverse integral

X-ray opacity measurements

Spectra extraction

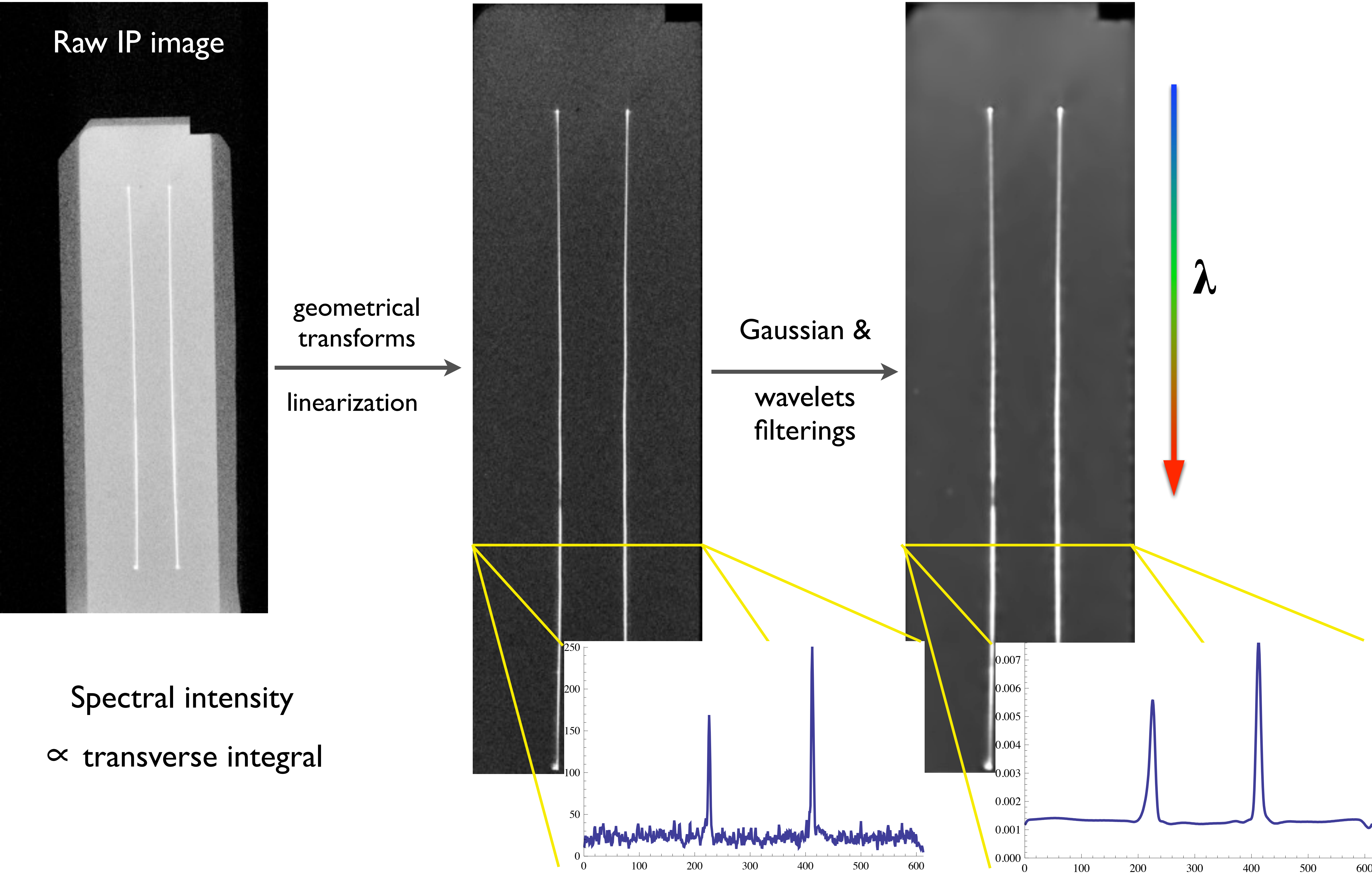

Raw IP image

geometrical transforms

linearization

Gaussian &

wavelets filterings

Spectral intensity

$\propto$ transverse integral

X-ray opacity measurements

Experimental absorption spectra

Iron

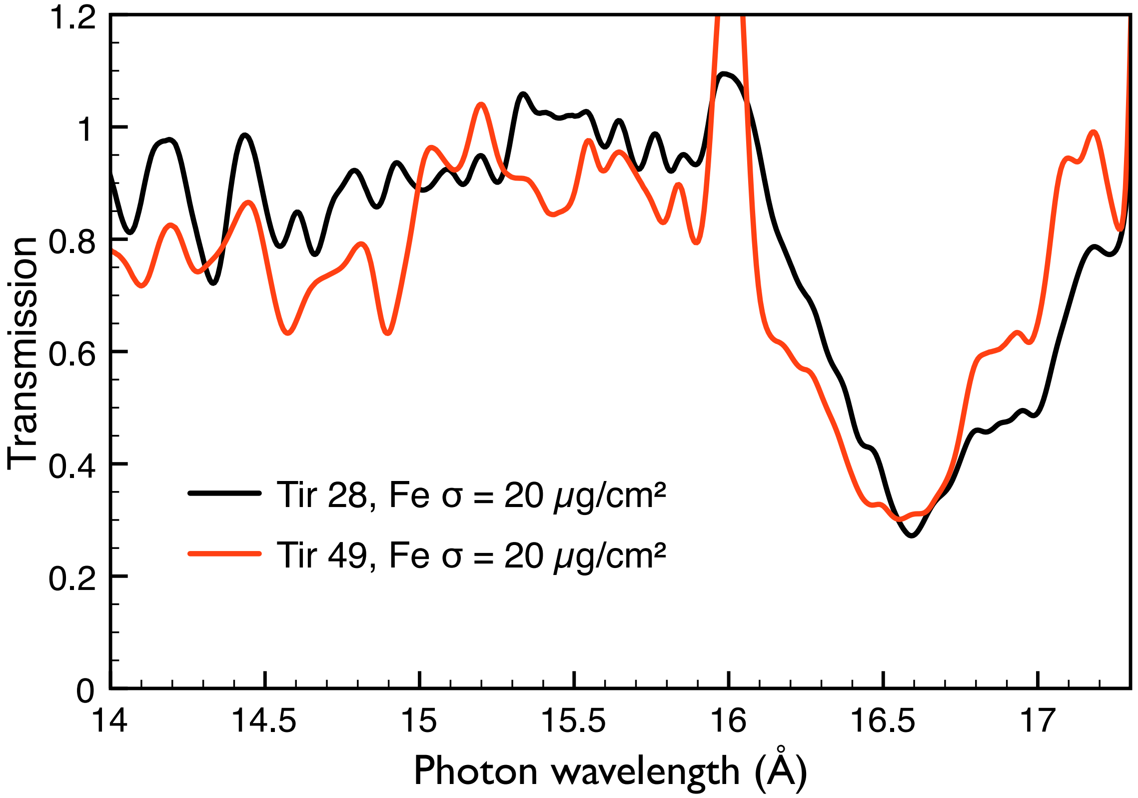

Copper

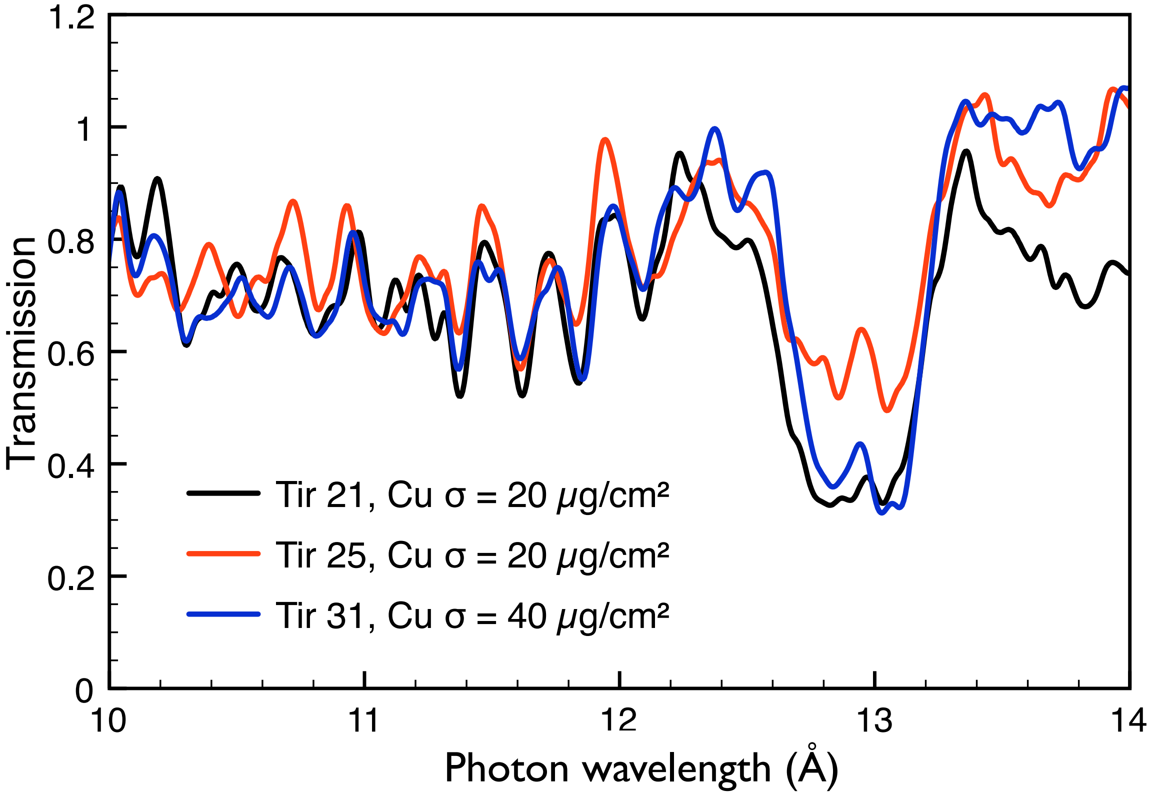

Nickel

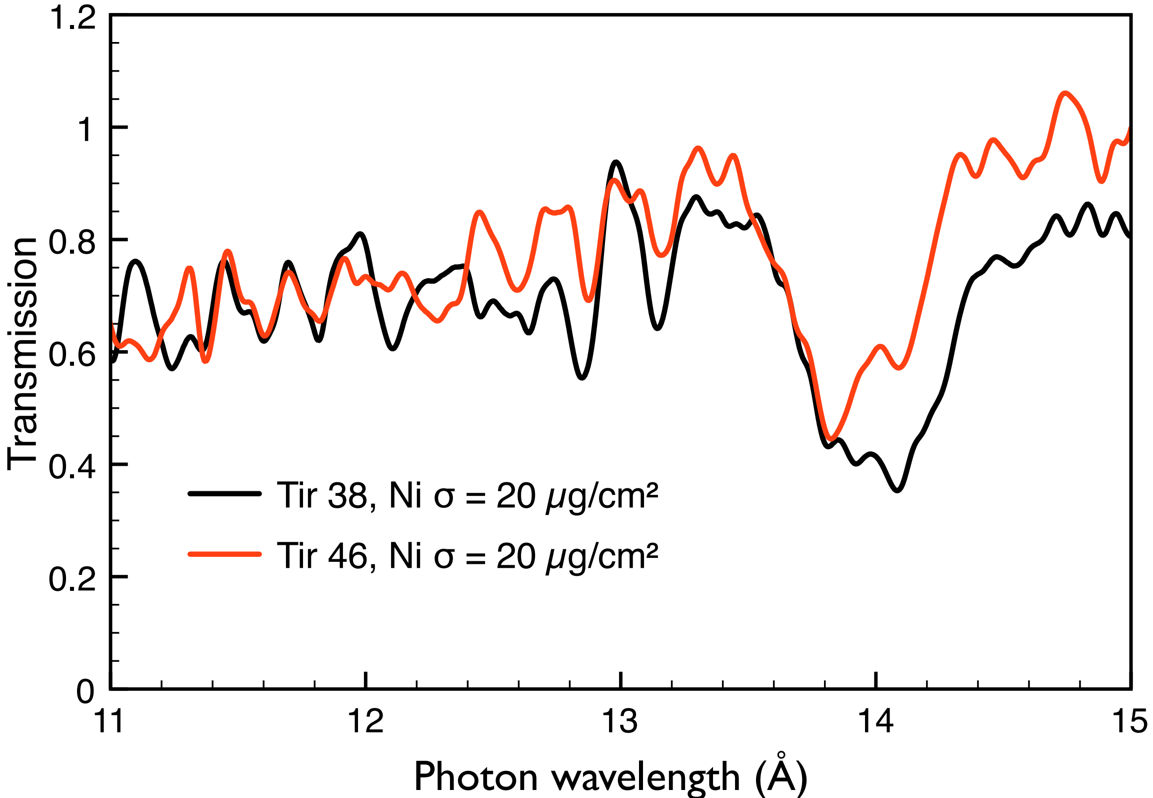

Loisel et al, HEDP, 5, 173, 2009

X-ray opacity measurements

Experimental absorption spectra

Iron

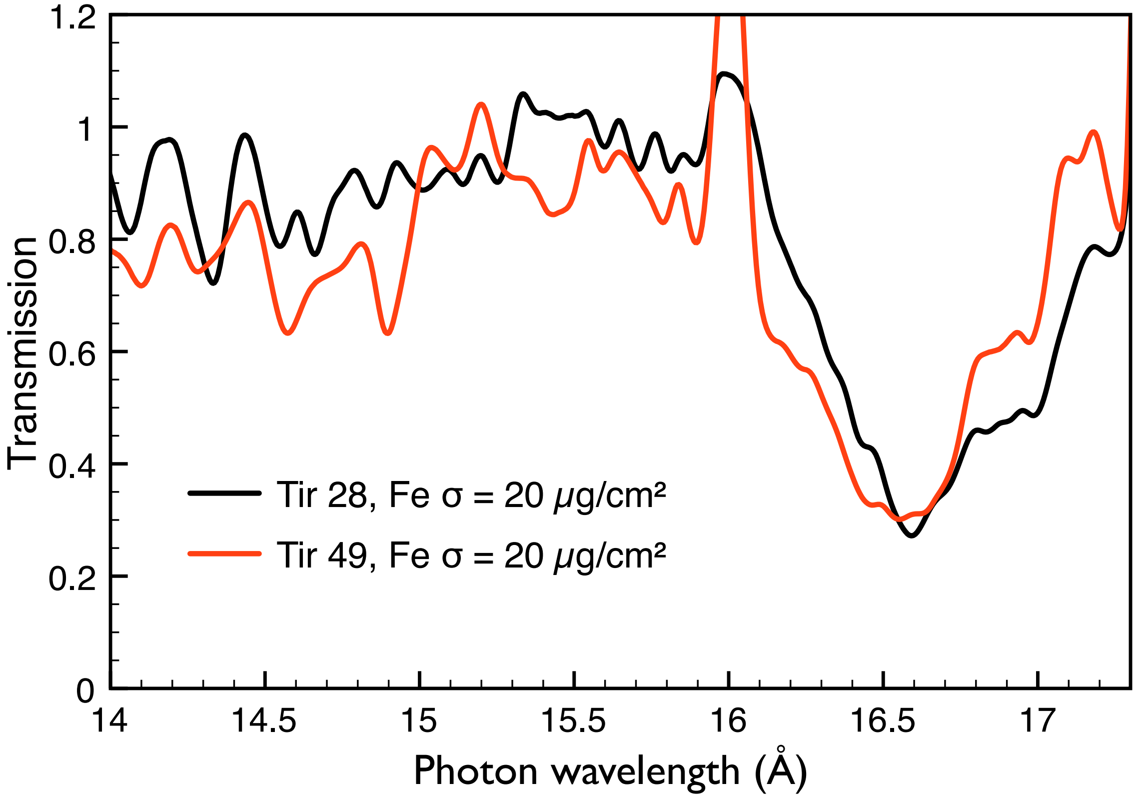

Copper

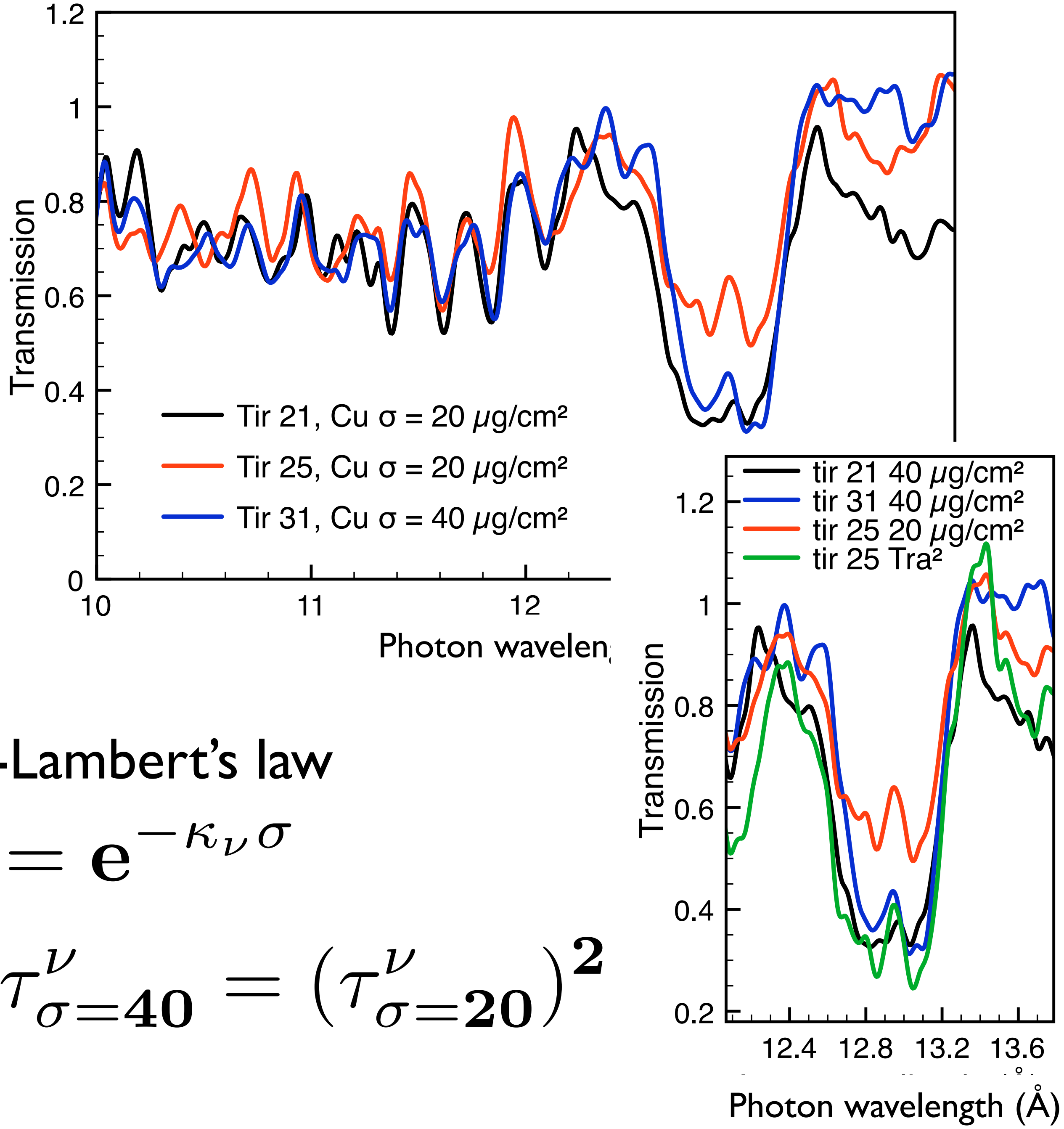

Nickel

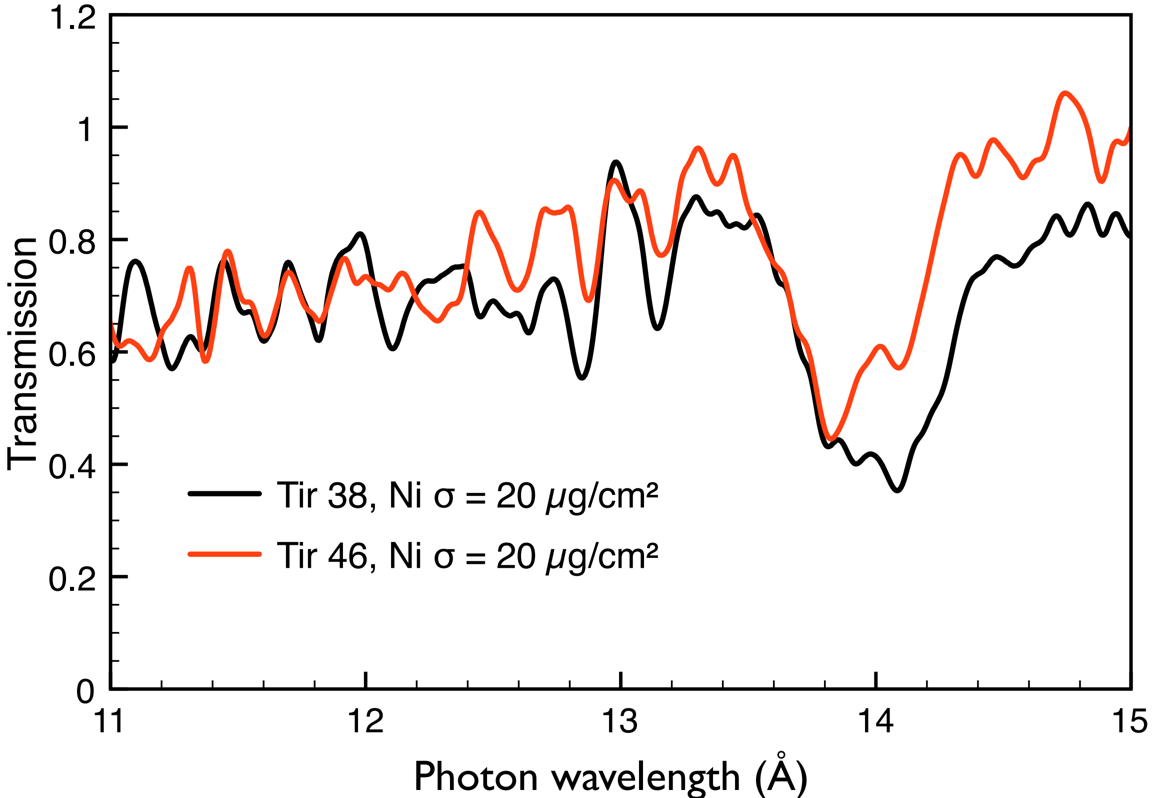

Beer-Lambert's law

$$\tau^{\nu}_{\sigma} = \mathbf{e}^{-\kappa_{\nu}\sigma}$$

$$\Rightarrow \tau^{\nu}_{\sigma=\mathbf{40}} = \left(\tau^{\nu}_{\sigma=\mathbf{20}}\right)^{\mathbf{2}}$$

Loisel et al, HEDP, 5, 173, 2009

X-ray opacity measurements

Simulation of plasma parameters

1D Radiation hydrodynamics computations FCI-1*. Input : micro-DMX estimates

Spatial profiles for the Iron opacity measurements (20 µg/cm²)

Time variations

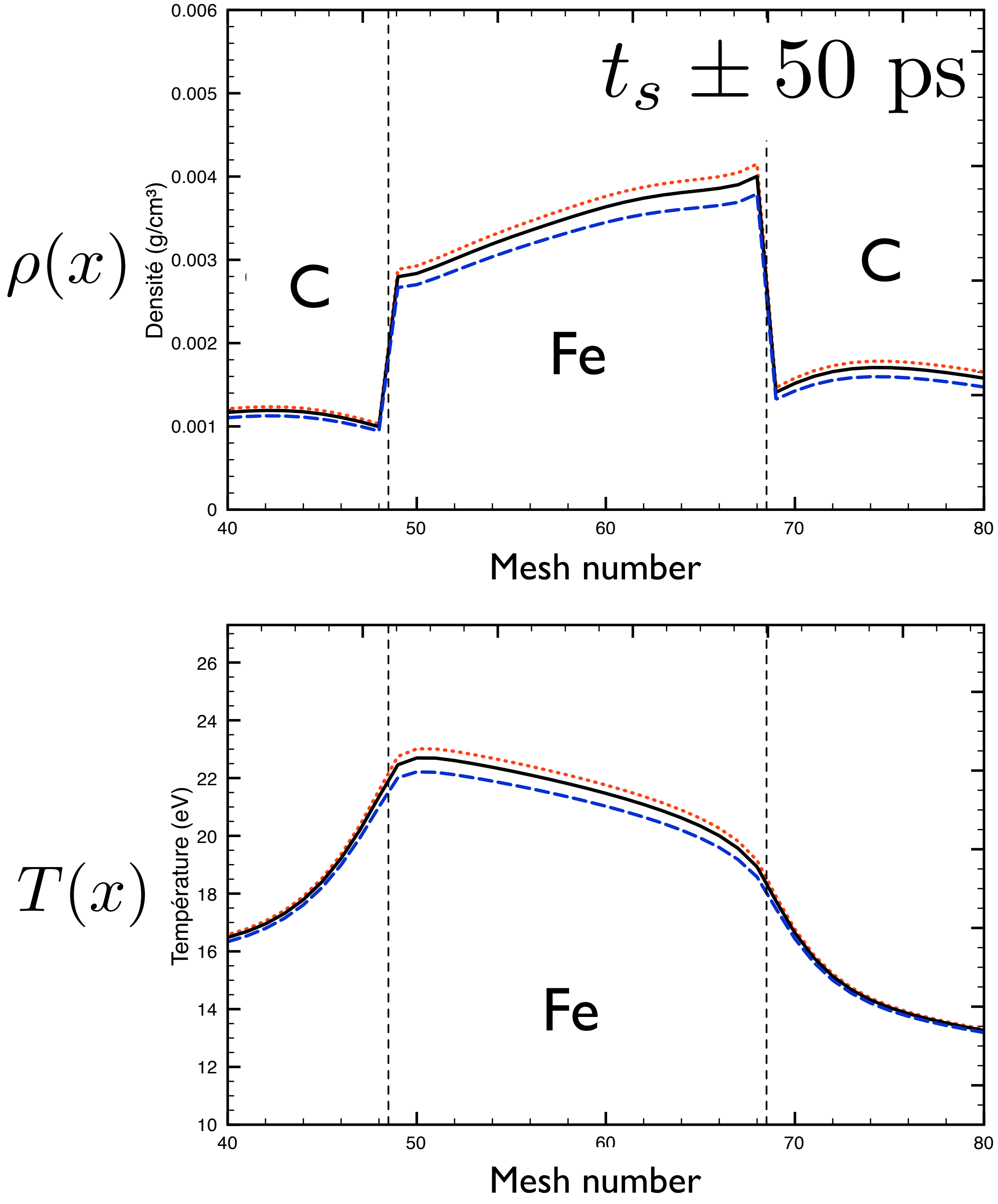

ρ=3.5±0.5 mg/cm³

T_e=21±2 eV

micro-DMX uncertainties

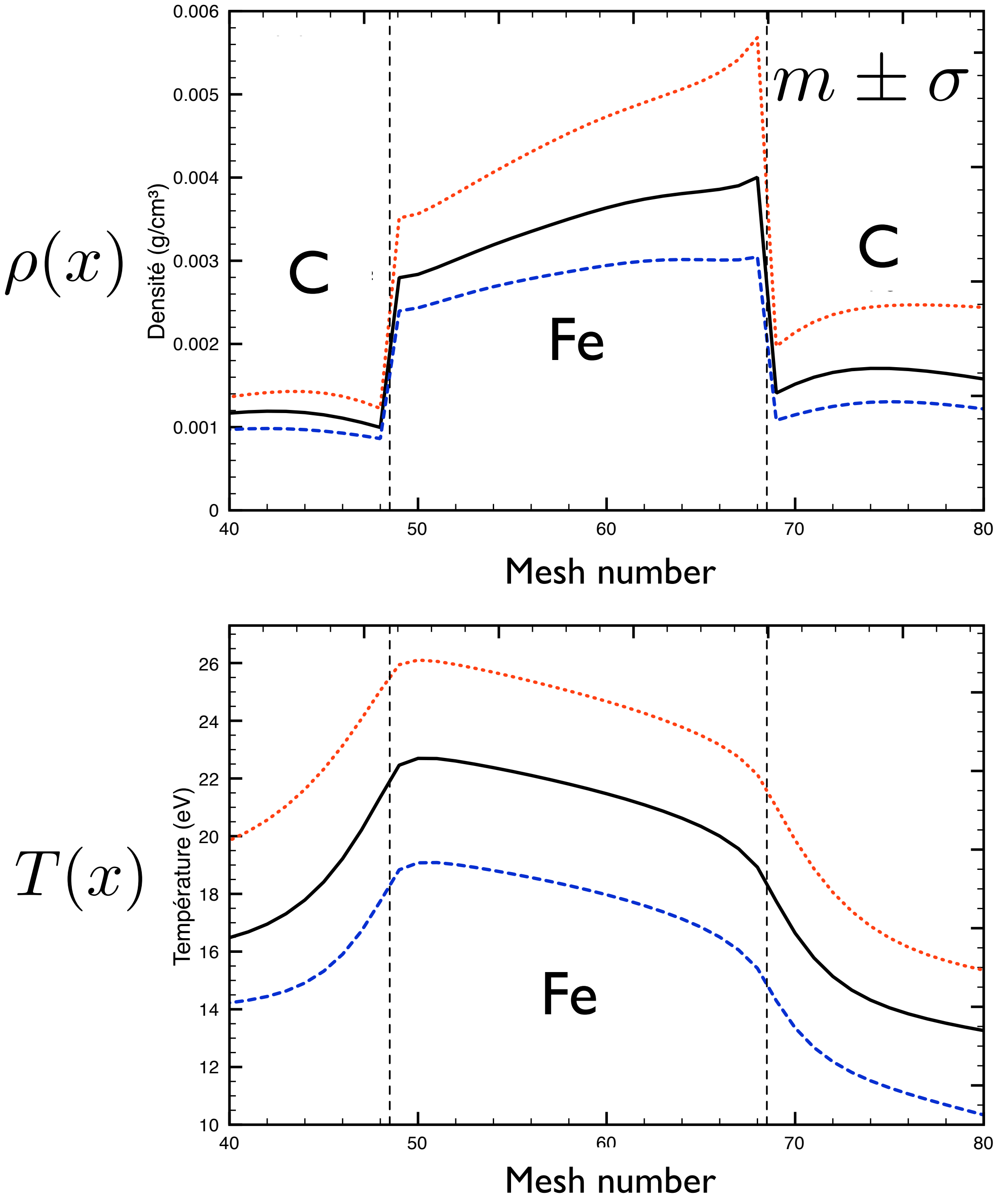

ρ=3.5±1.5 mg/cm³

T_e=21±6 eV

* *Schurtz et al, PoP 2000*

X-ray opacity measurements

Analysis : statistical computations SCO*

Iron

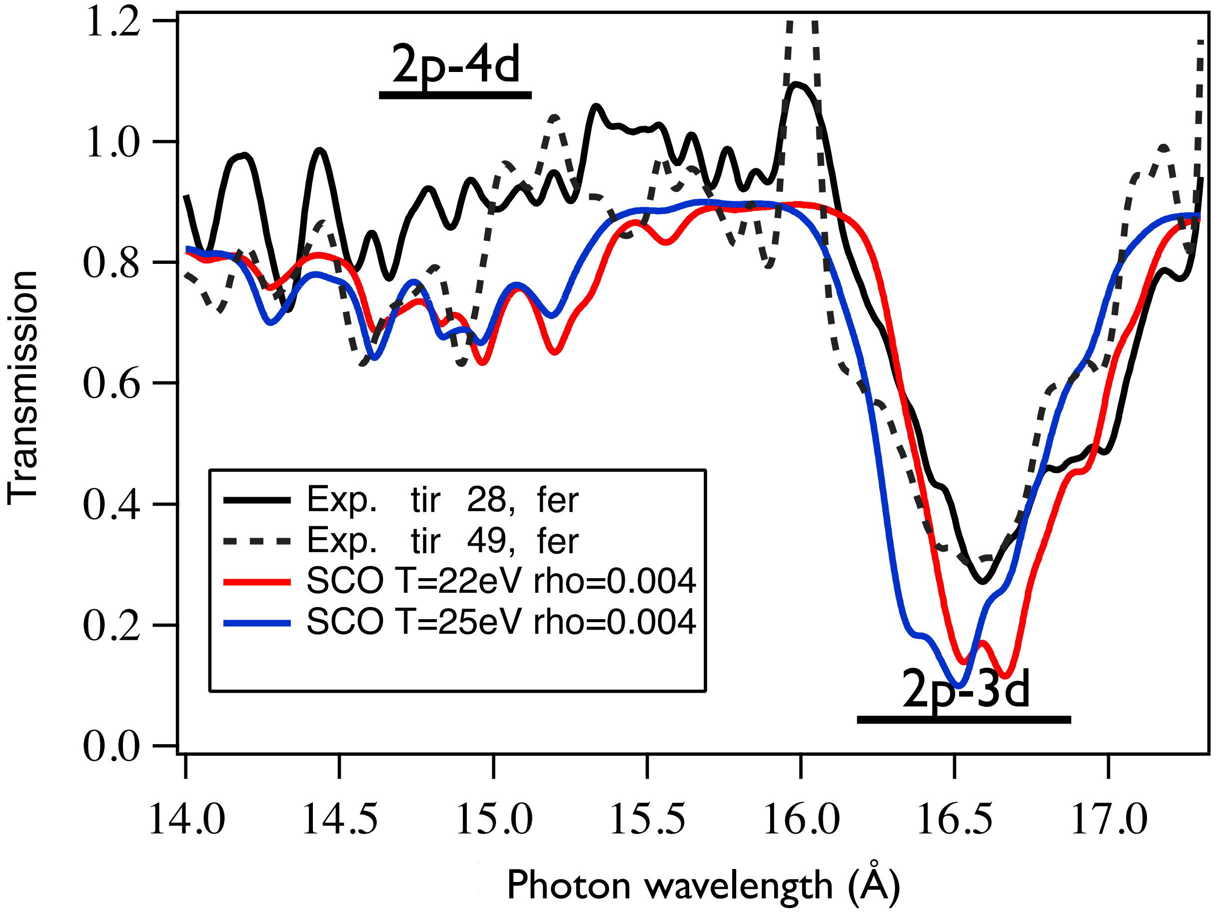

Nickel

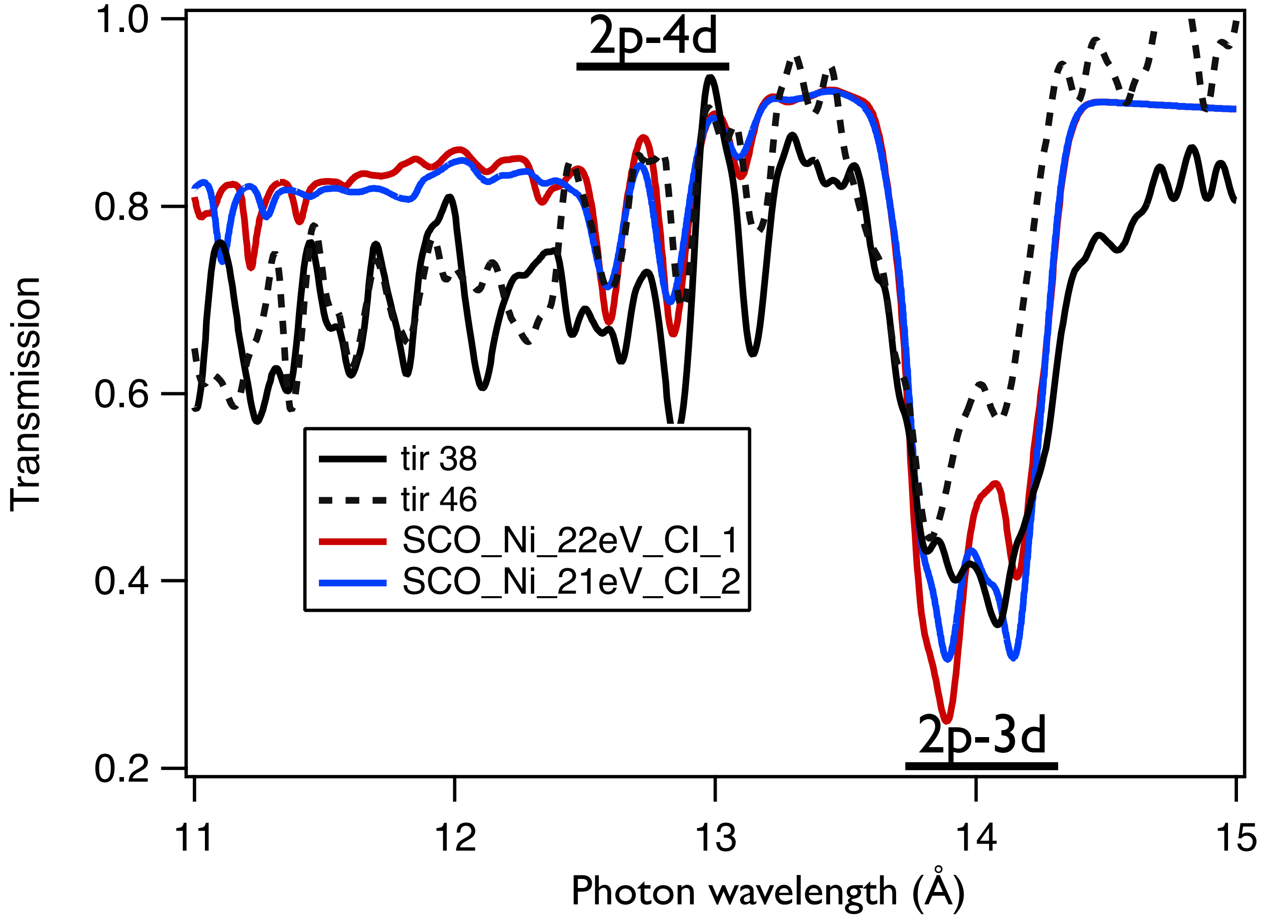

Blenski ... Loisel... et al., to be published

* *SCO : T. Blenski et al. 2000*

X-ray opacity measurements

Analysis : detailled computations HULLAC*

Iron

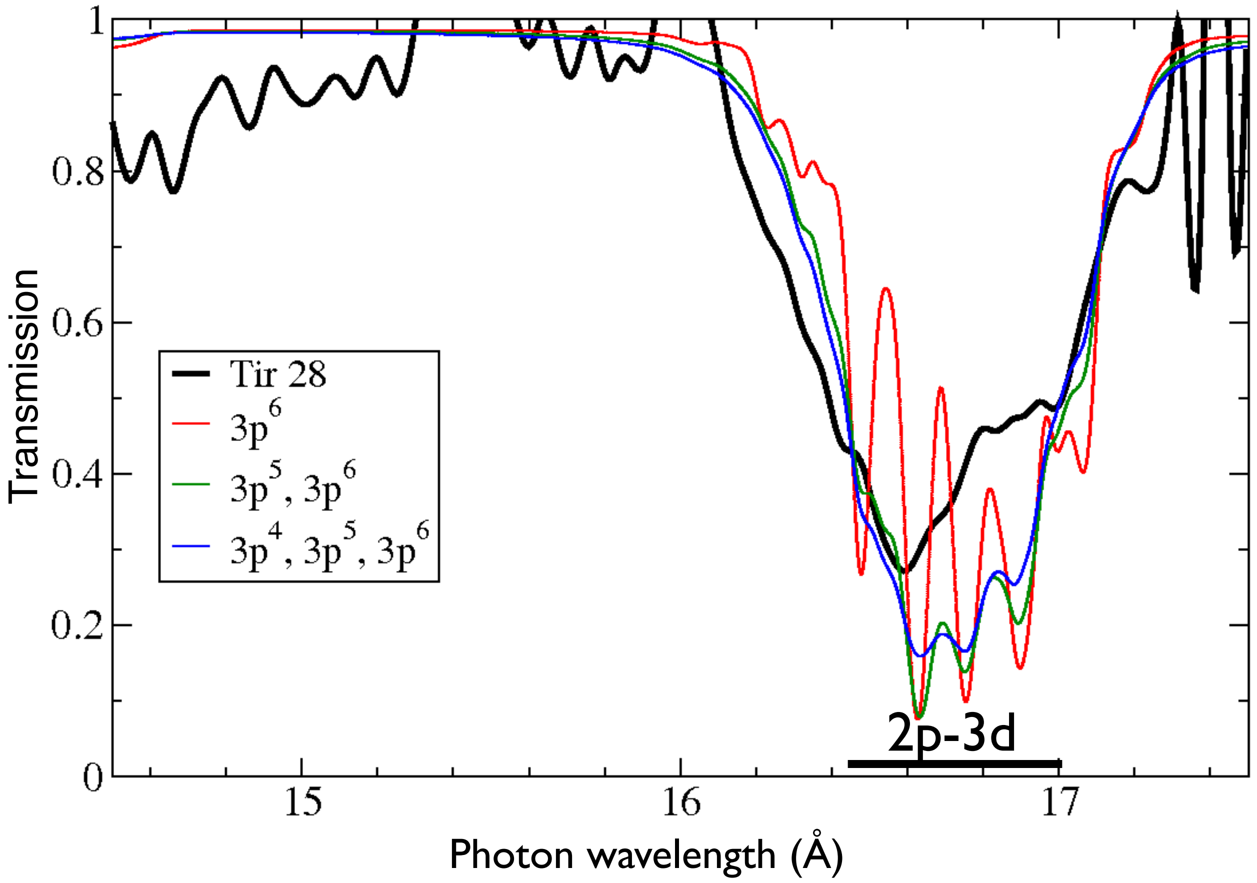

Nickel

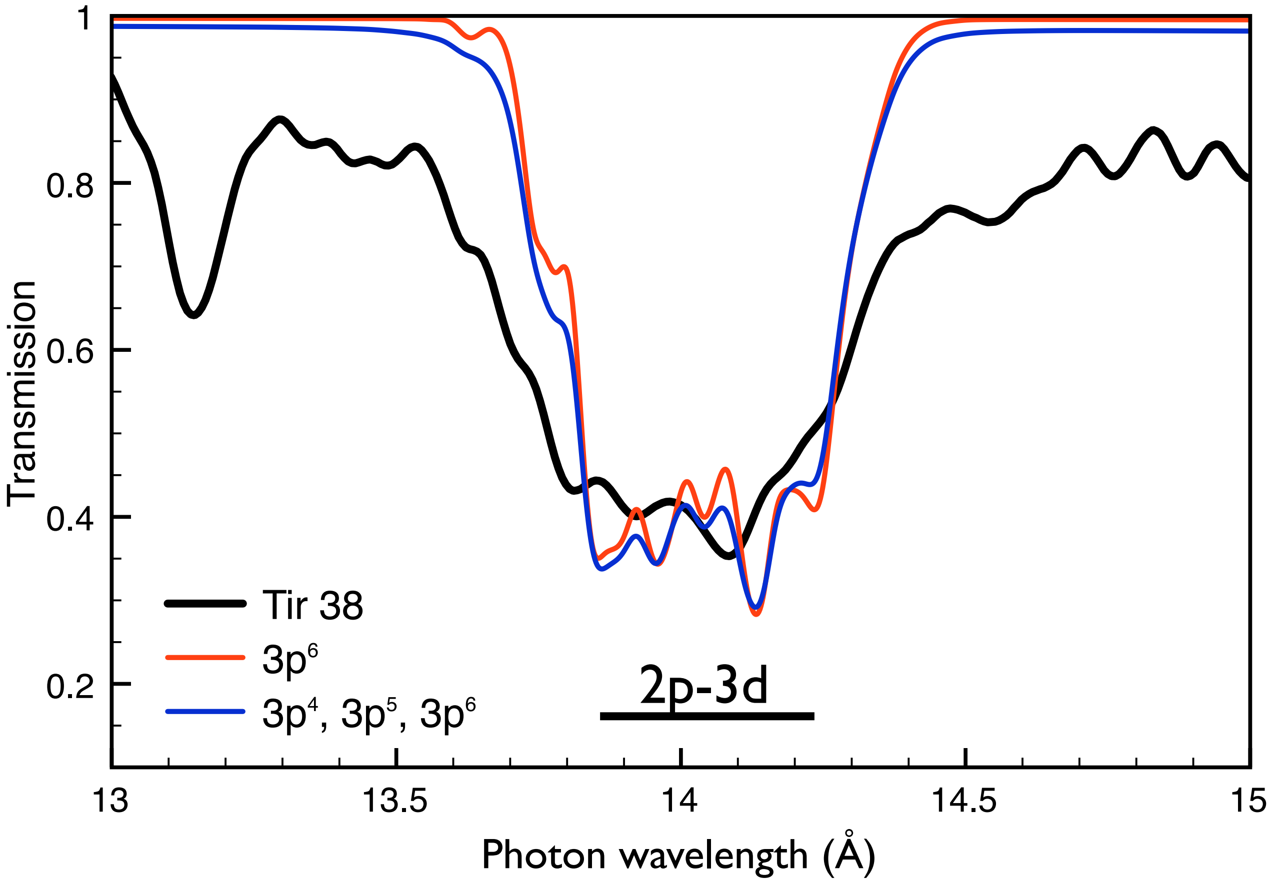

- ➡ Effect of the opening of the spectactor sub-shell 3p on the main structure 2p-3d
- ➡ Important for Iron and diminishes with increasing Z

Poirier et al., to be published

---

* *HULLAC : Bar-Shalom et al., 2001*

X-ray opacity measurements

Analysis : case of copper

SCO

shots 31 et 21
40 μg/cm^{2}

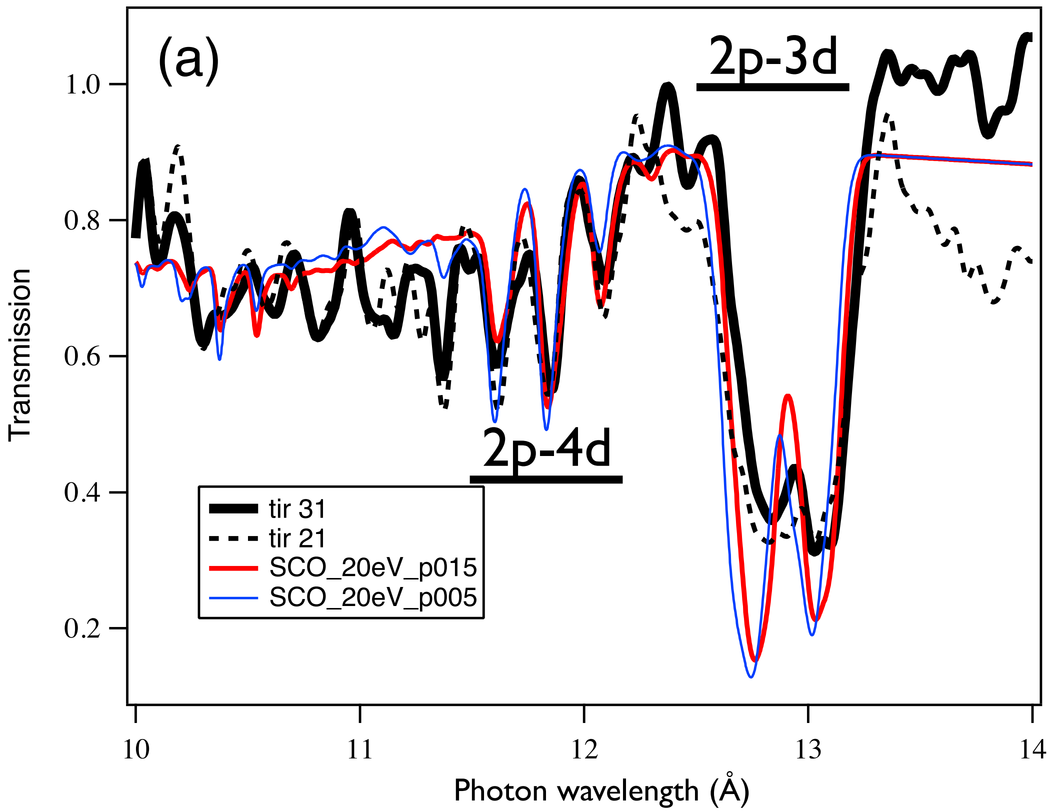

HULLAC

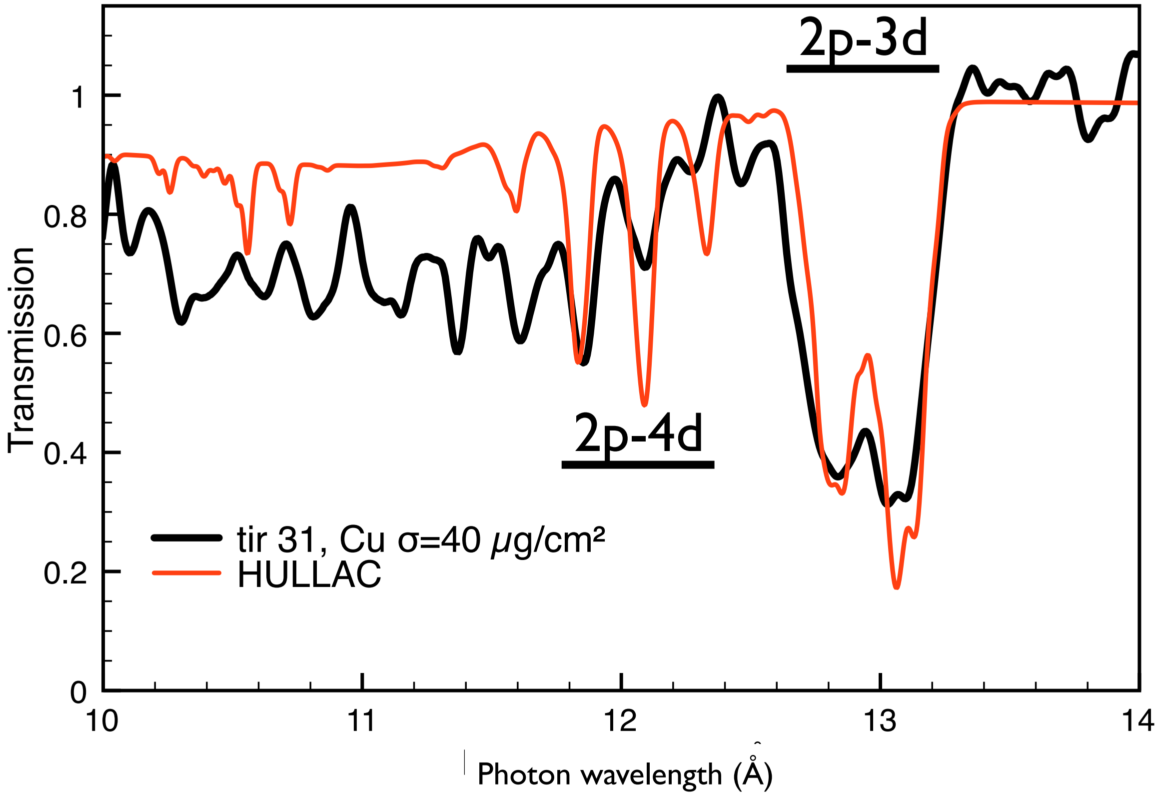

shot 25
20 μg/cm^{2}
shot 31
40 μg/cm^{2}

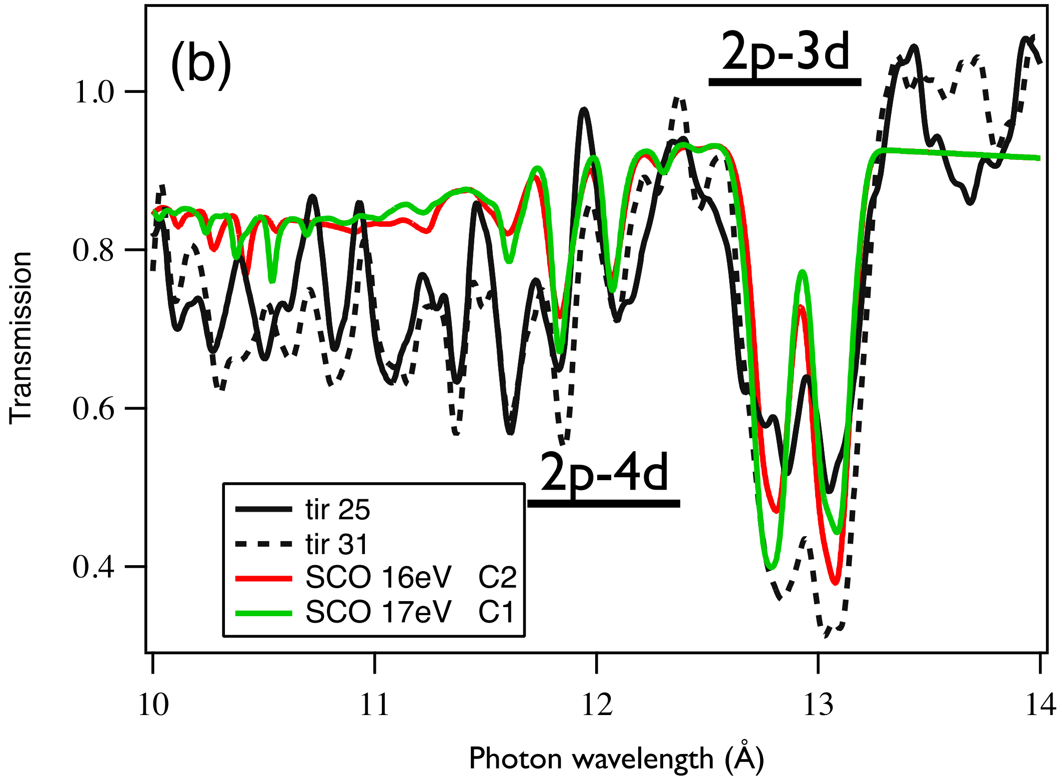

X-ray opacity measurements

2009 - BaF_2, Sm, Gd & Ho

➡ 3d-4f transitions evolutions with respect to the atomic number (Z~60)

Theory

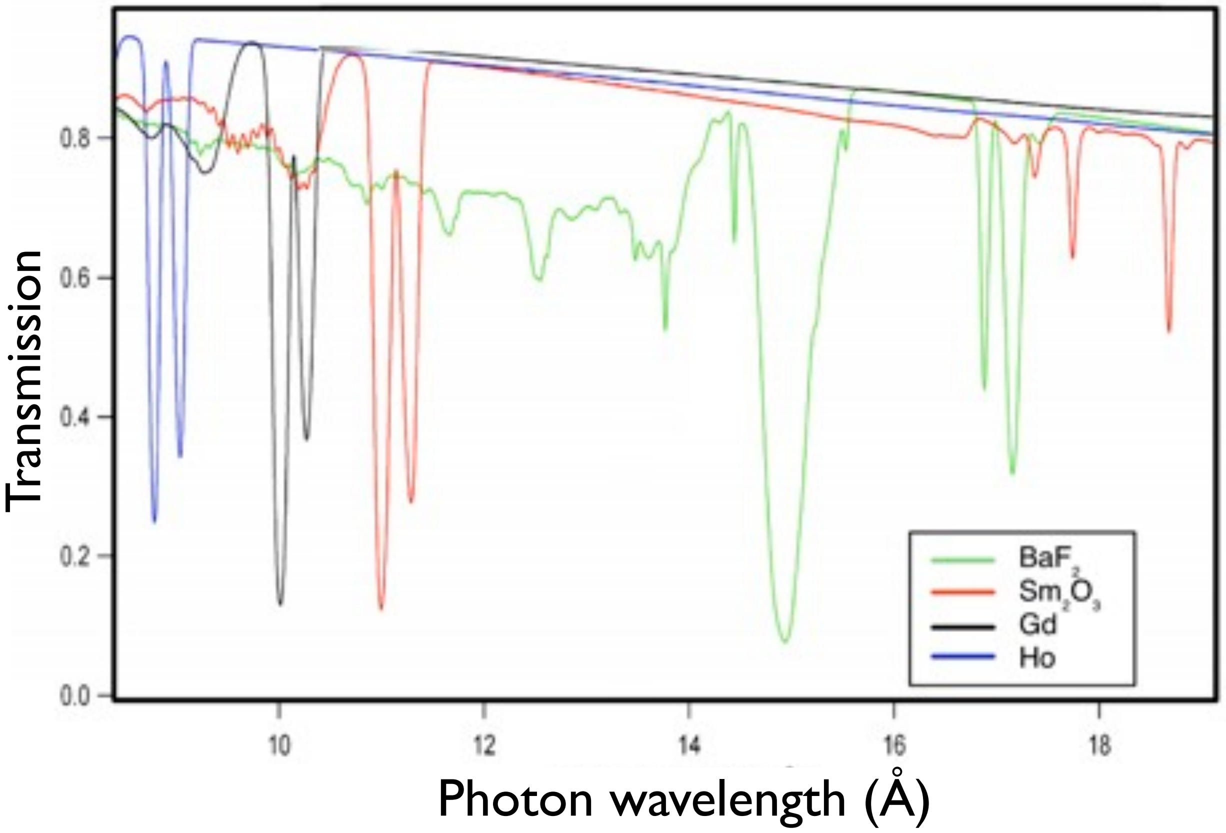

Experiment

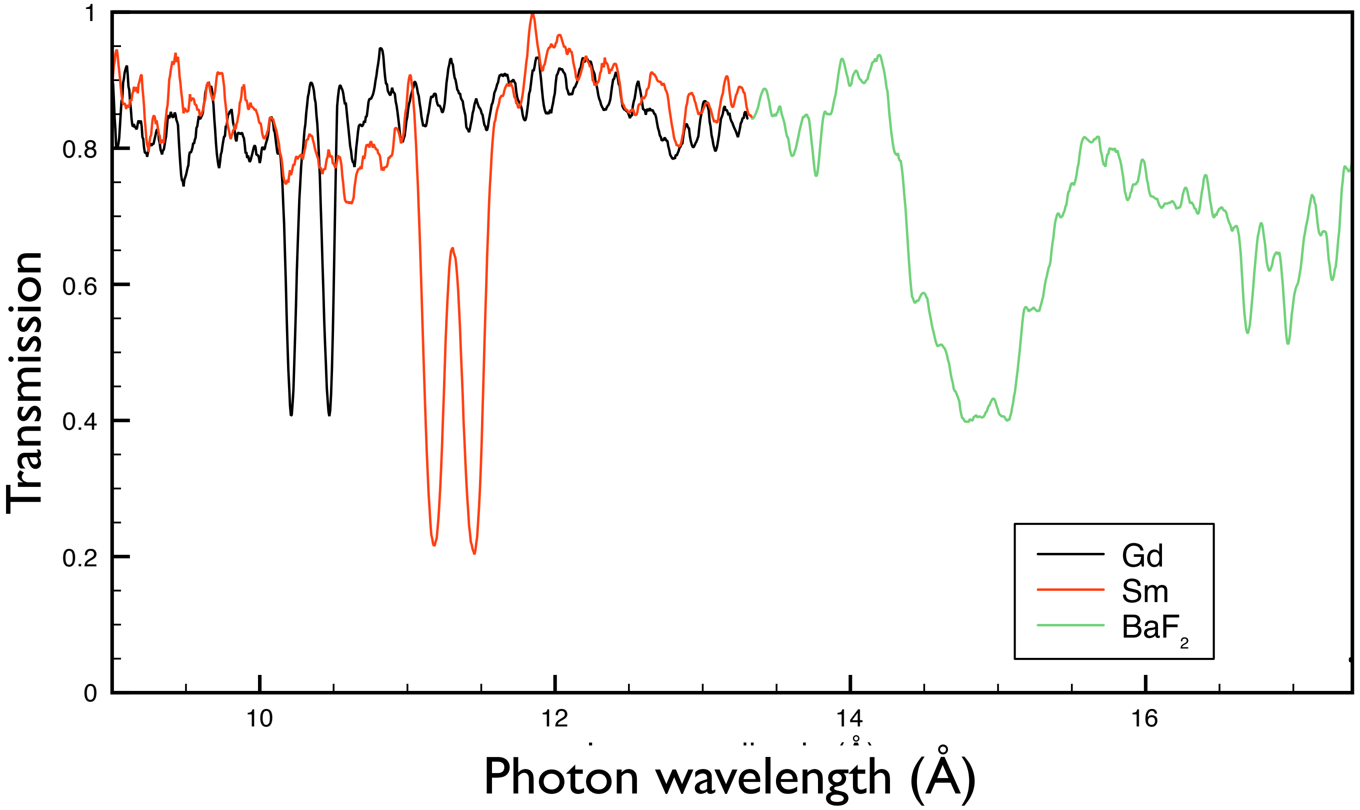

SCO, T. Blenski et al. 2000

XUV opacity measurements
Double hohlraum setup

β-Cephei opacities

Comparisons of opacity profiles using OP and OPAL data along a $10\mathrm{M}_\odot$ β-Cephei temperature profile

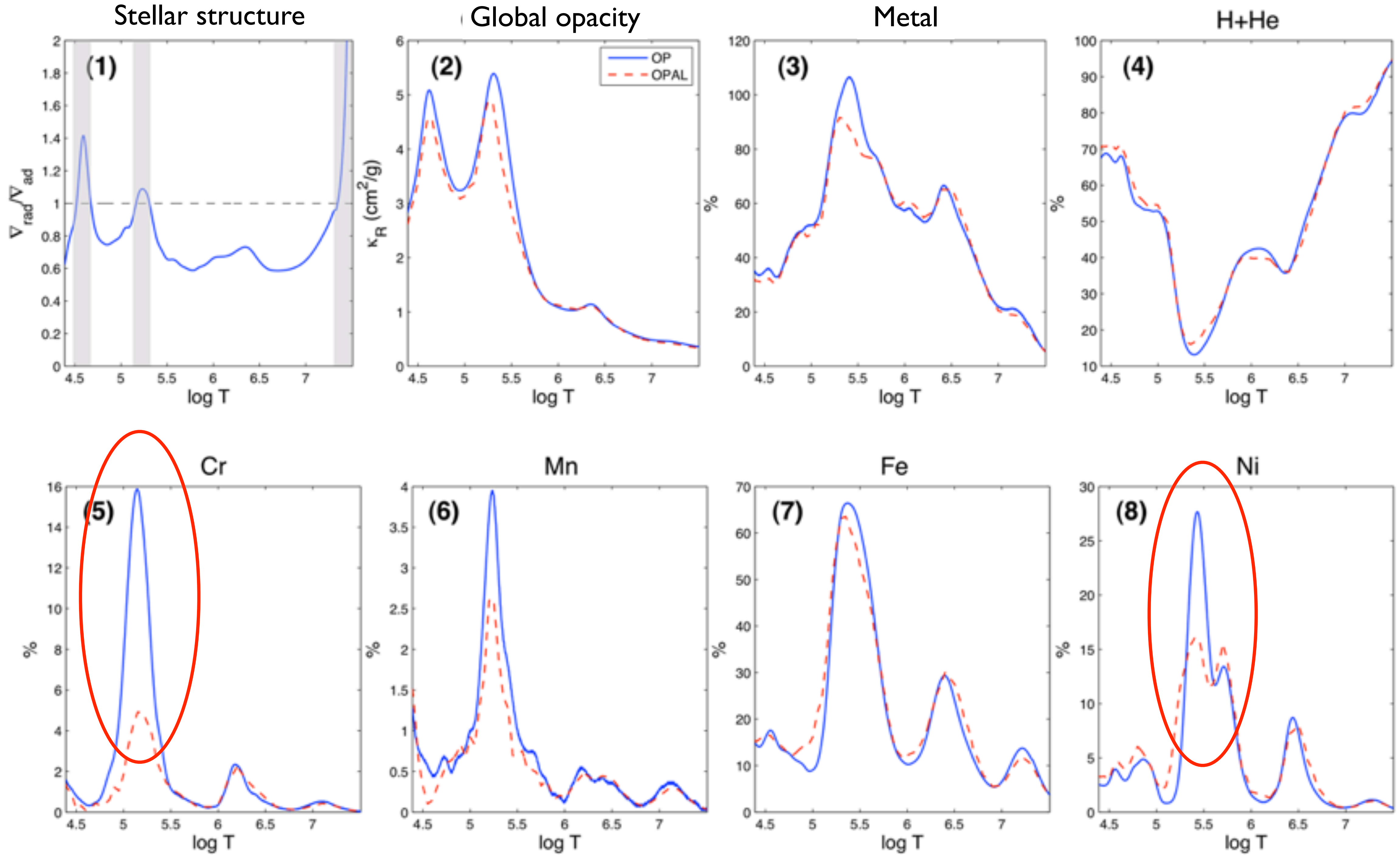

➡ High difference at the Z-bump location responsible for β-Cephei pulsations, in particular for Nickel and Chromium, less for Iron @T~15.3 eV $\rho \sim 3.5 \times 10^{-6}$ g/cm^3

Turck-Chièze, Loisel et al, Astrophys. Space Sci., 2011

Radiative levitation

➡ differences between OP and OPAL in radiative acceleration for conditions encountered in β-Cephei atmosphere (up to 50% in the case of Fe at max. opacity)

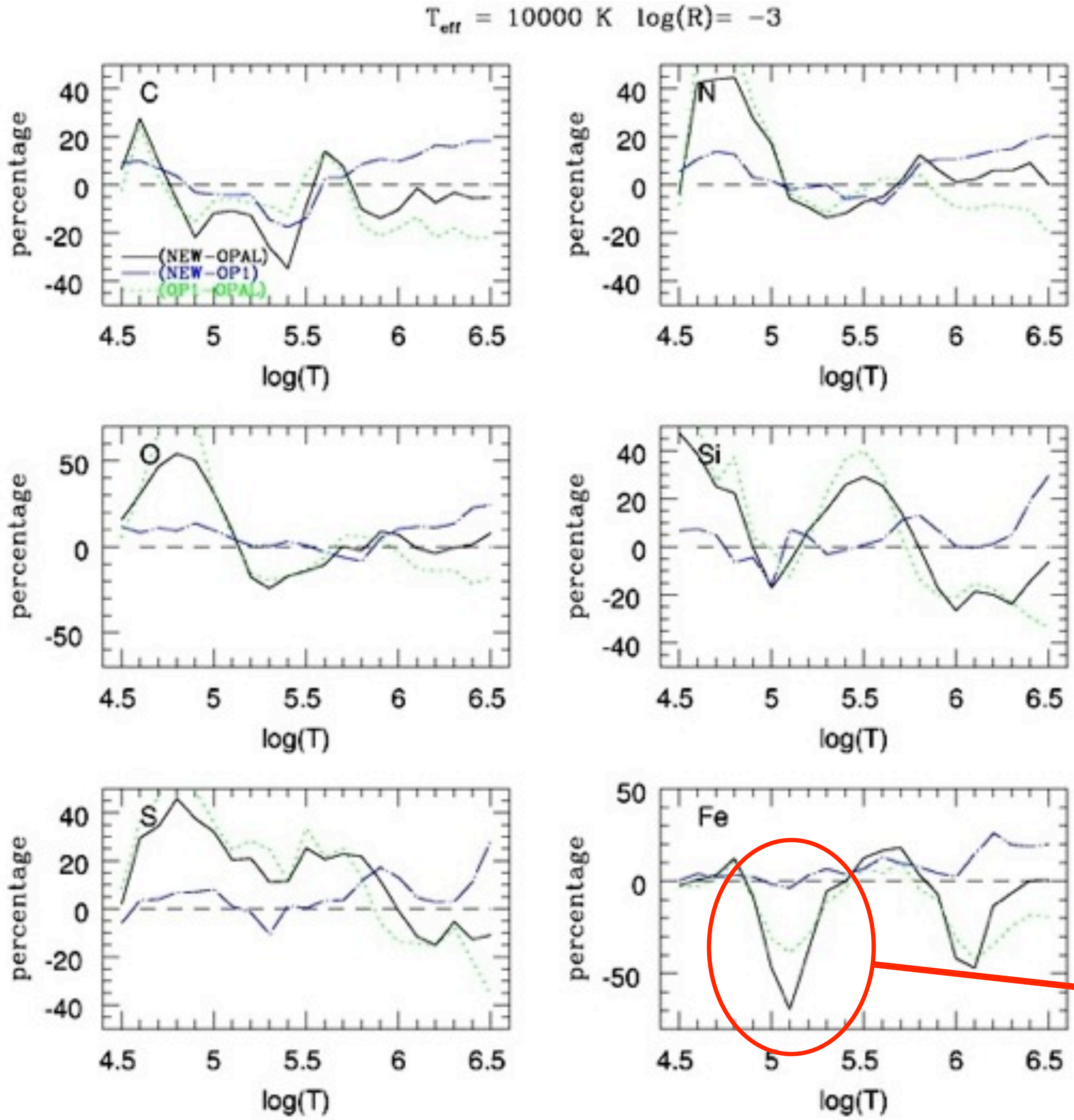

Relative differences per elements (OP-OPAL)/OPAL, *From Delahaye et al. 2005*

Acceleration uses elemental spectra uses elemental spectral opacity

$$gr(k) = \frac{F}{c}\frac{\overline{m}}{m_k}\kappa_R \int \frac{\kappa_\nu(k)}{\kappa_\nu} f_\nu d\nu$$

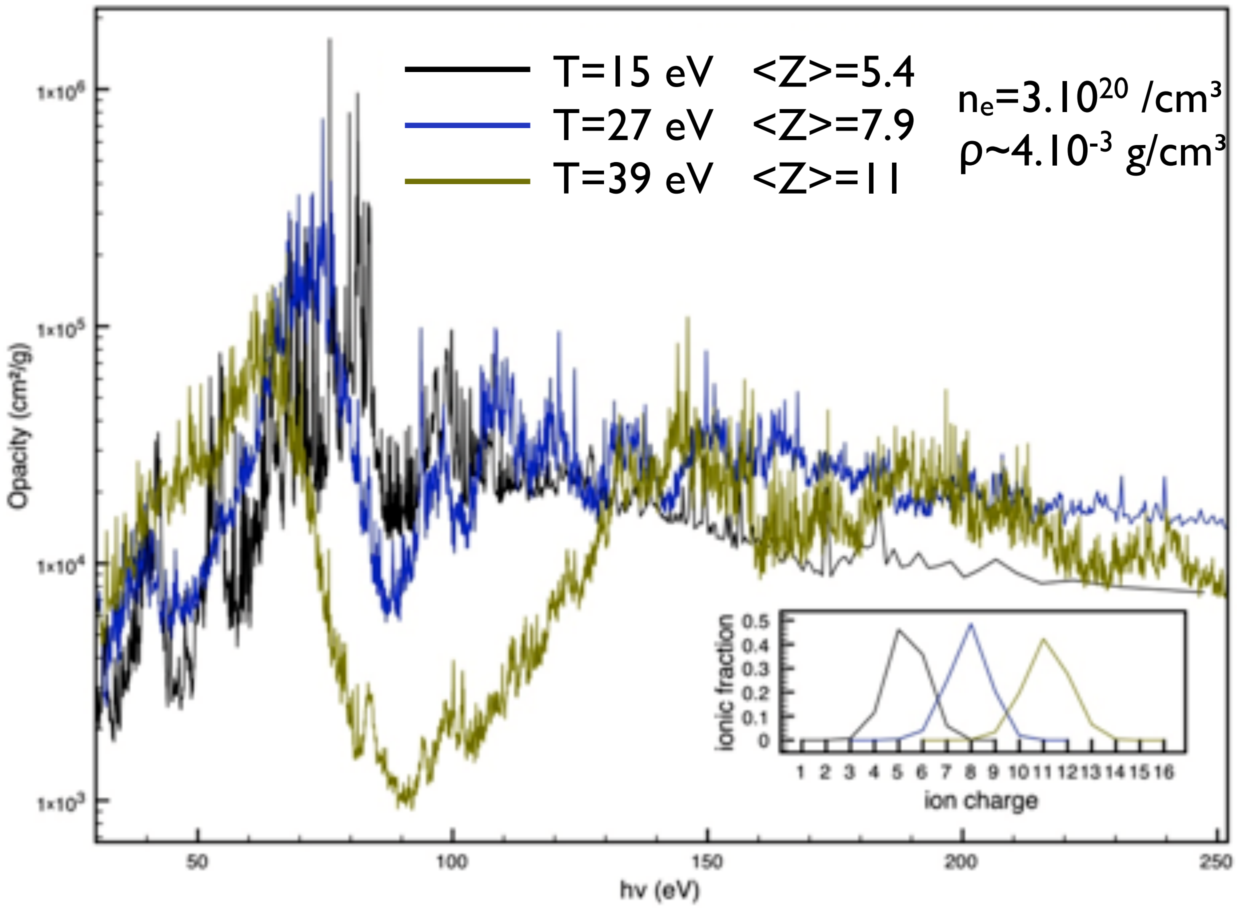

→ Strong sensibility with temperature

XUV opacity measurements

Plasma conditions

➡ Ionization conditions of Iron similar between the « β-*Cep*» case :

15.3 eV - 200 000 K - 3.5×10^{-6} g/cm^3

and experiment

27.3 eV - 400 000 K - 3.4×10^{-3} g/cm^3

<Z>~8.5

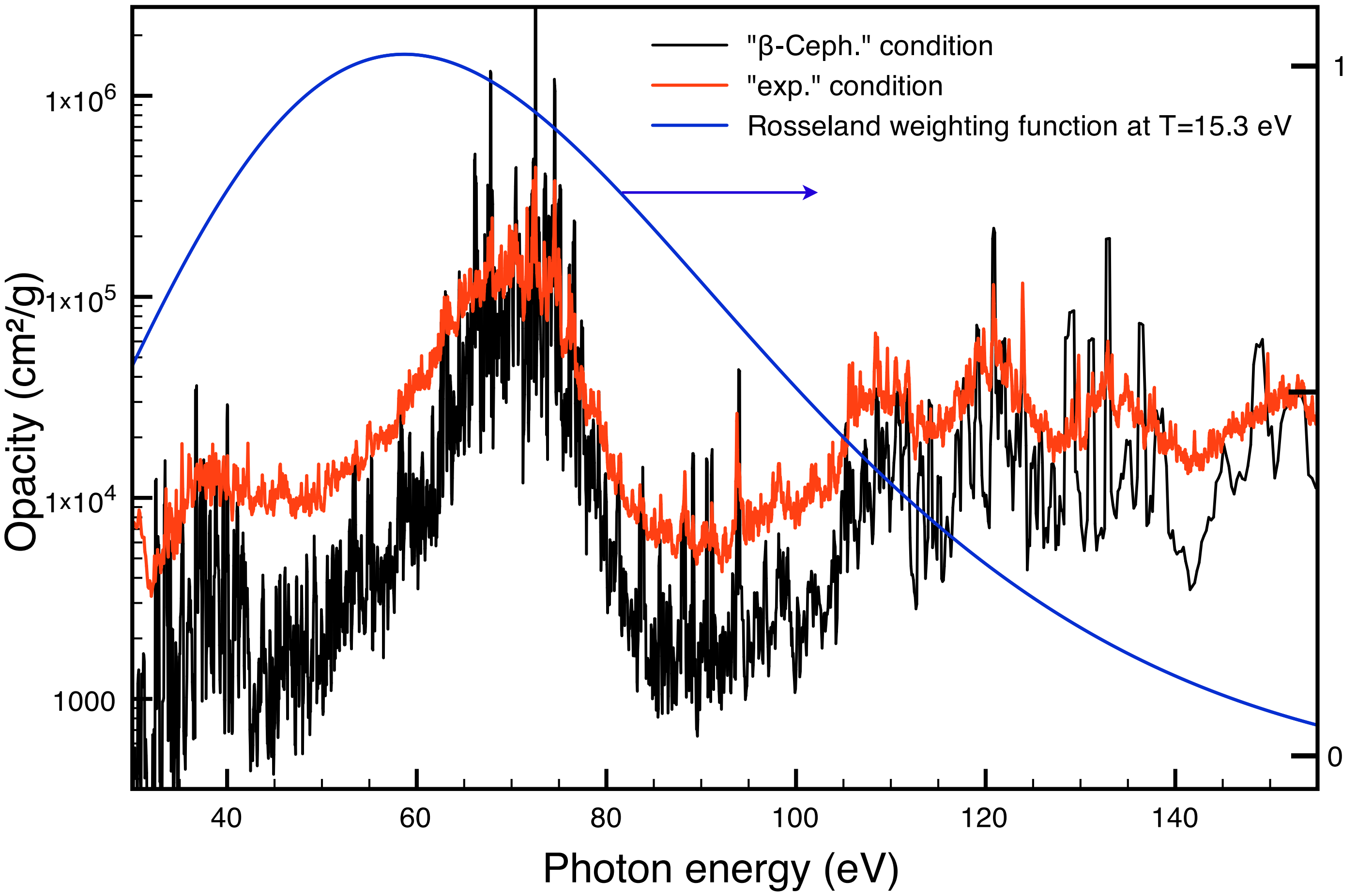

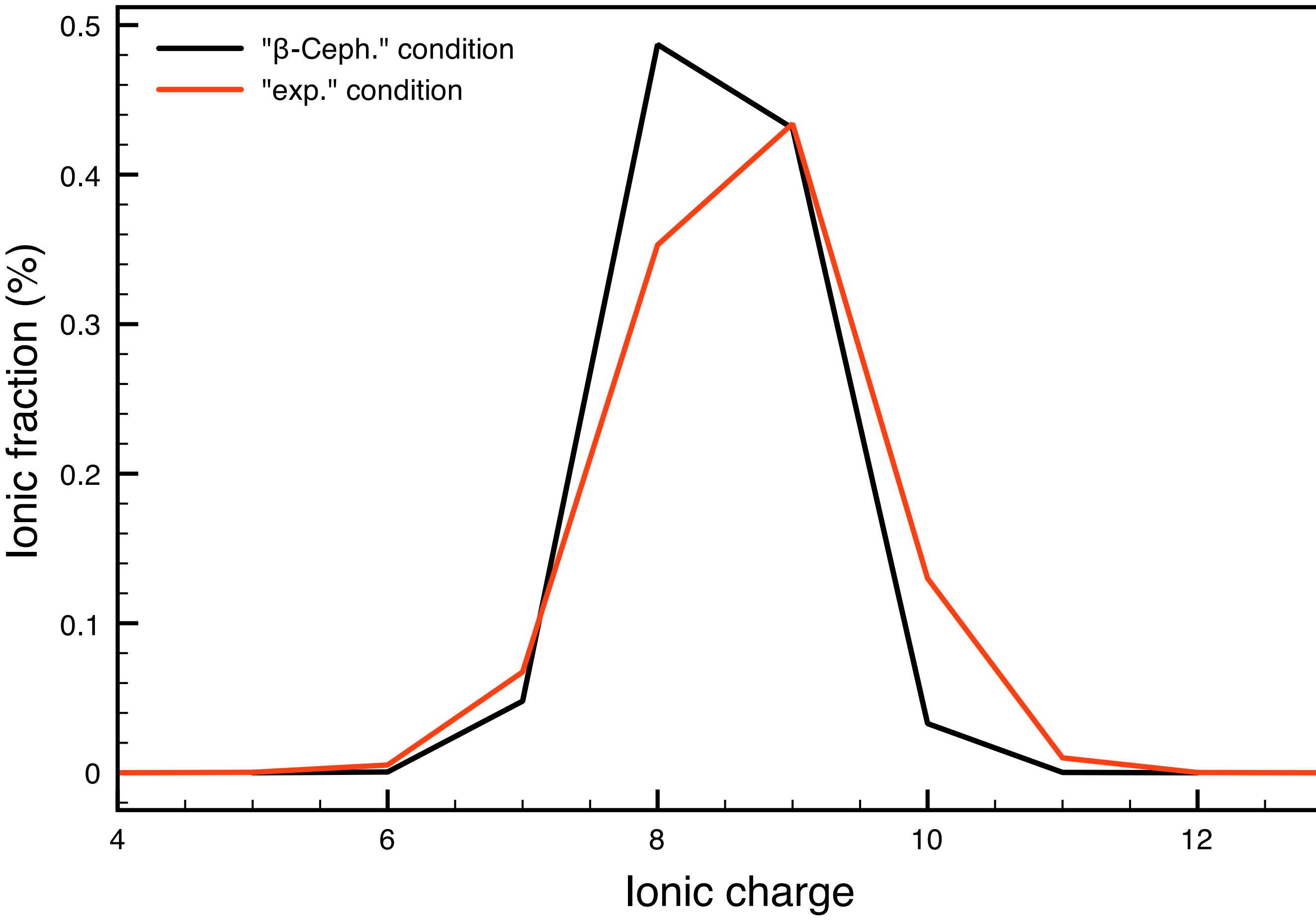

XUV opacity measurements

Theoretical predictions

Nickel transmission - 15 µg/cm² -Te=15.3, 27.3 et 38.5 eV

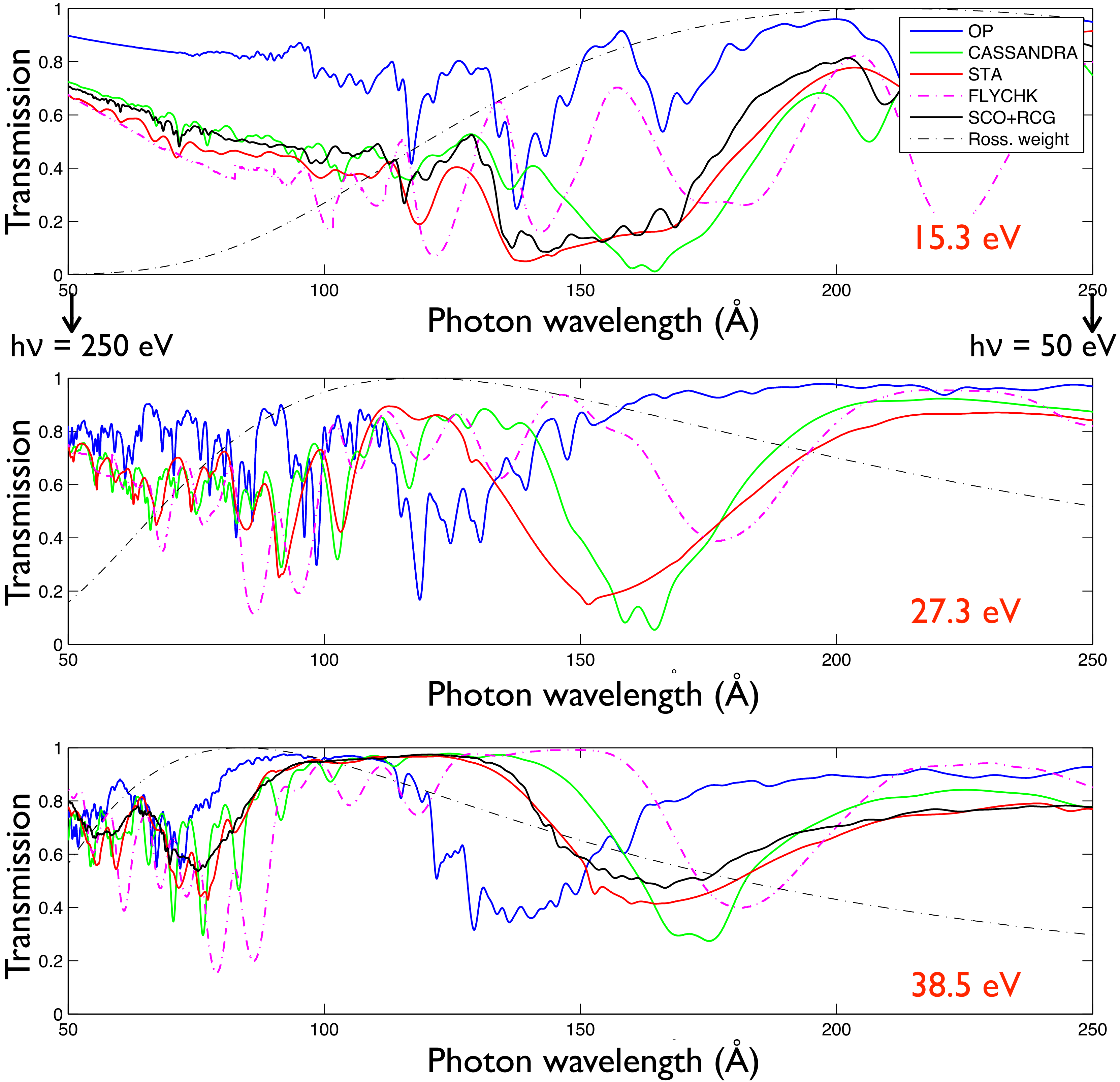

XUV opacity measurements

Heating using a double cavity

Targets

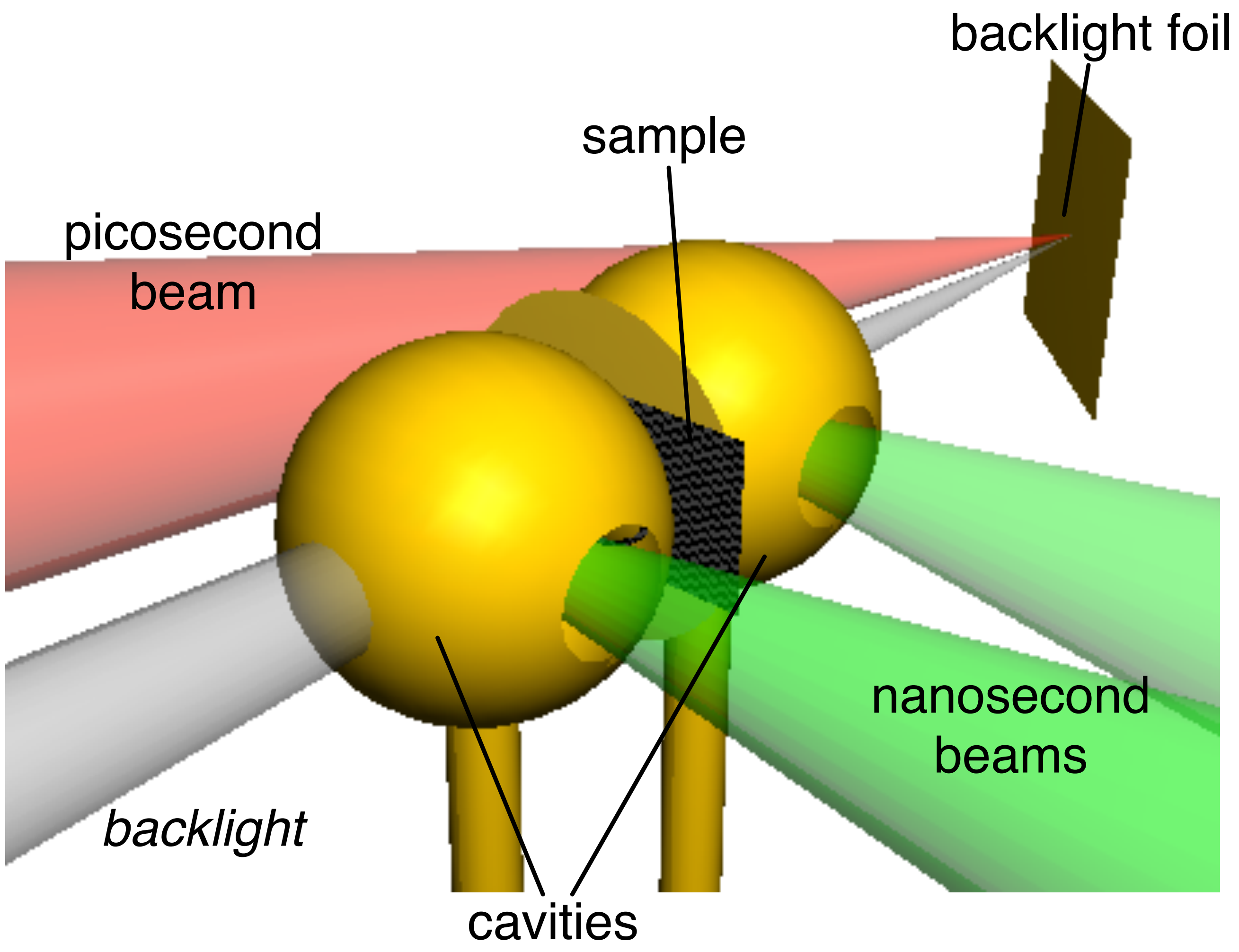

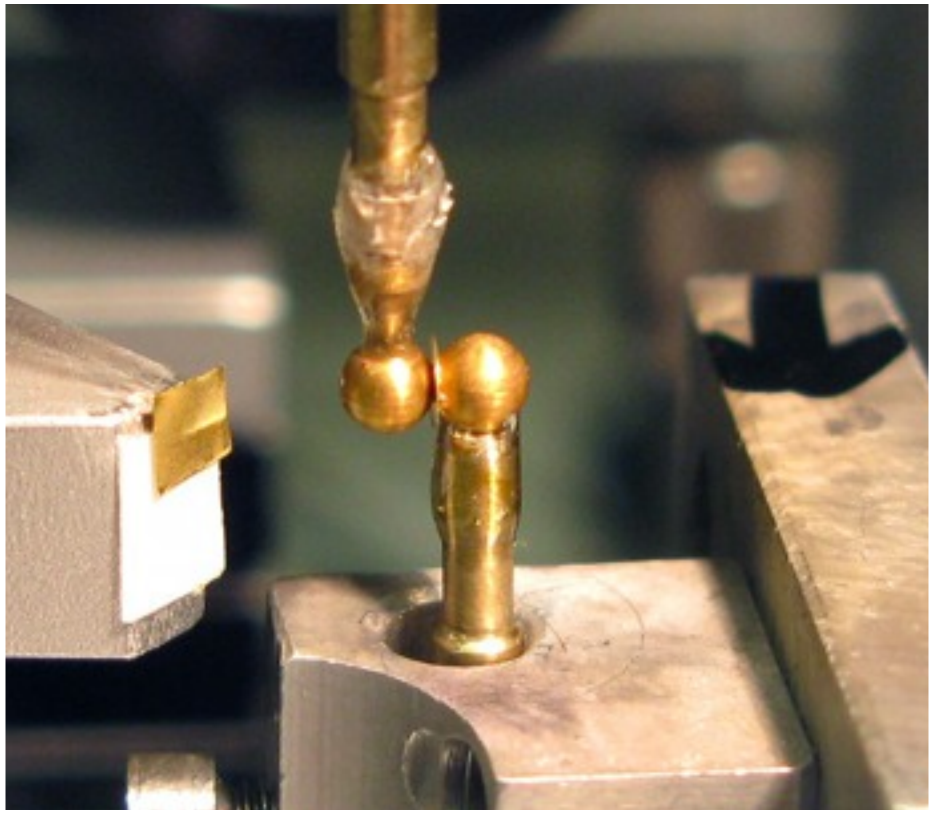

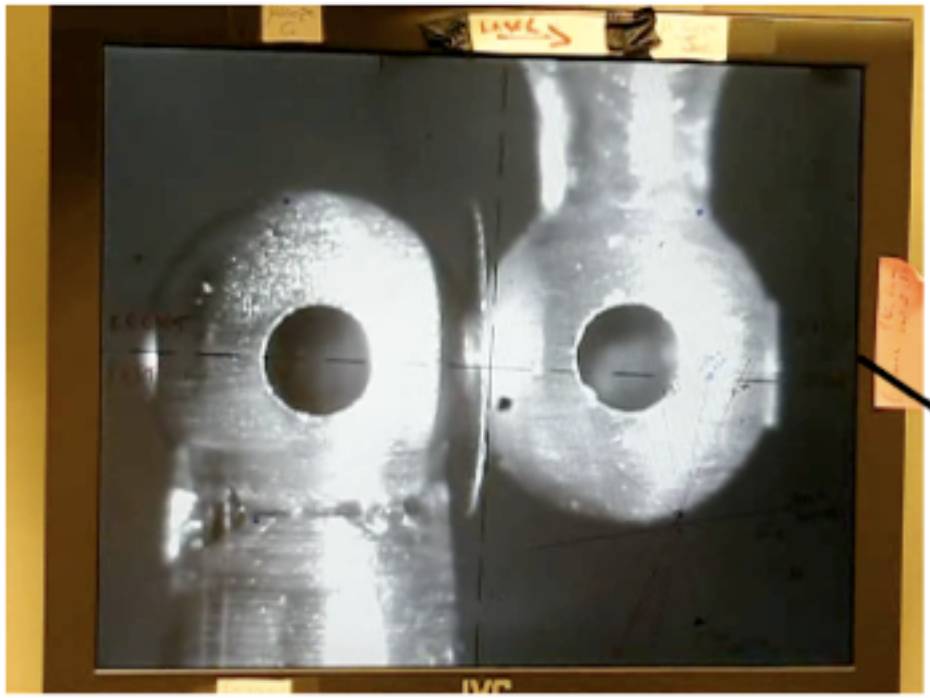

micro-DMX

XUV opacity measurements

Heating using a double cavity

Laser split

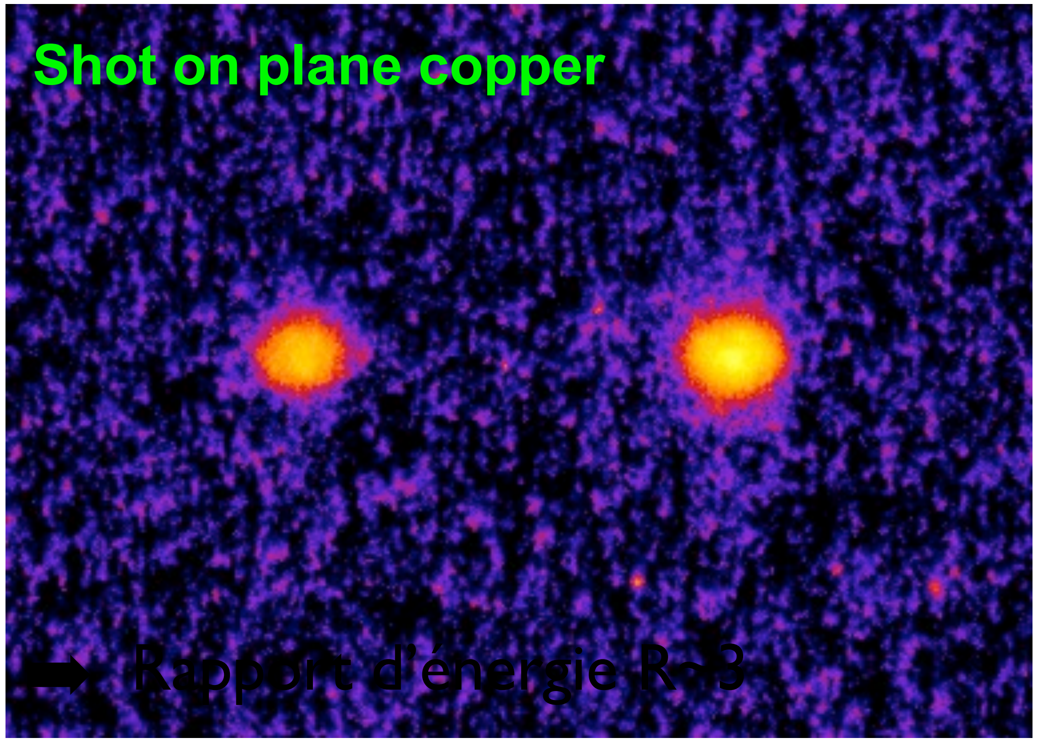

Shot on plane copper

➡ Rapport d'énergie R~3

Unfiltered pinhole camera gives:
1) X-ray energy ratios between «sub-beams»
2) their entry in cavities

Ratio of X-ray energy between cavities (1:right, 2:left)

→conversion rate E_X/E_L in the present laser regime (25-250 J, 600 ps, Φ 400 μm) on Cu & Au are nearly constant

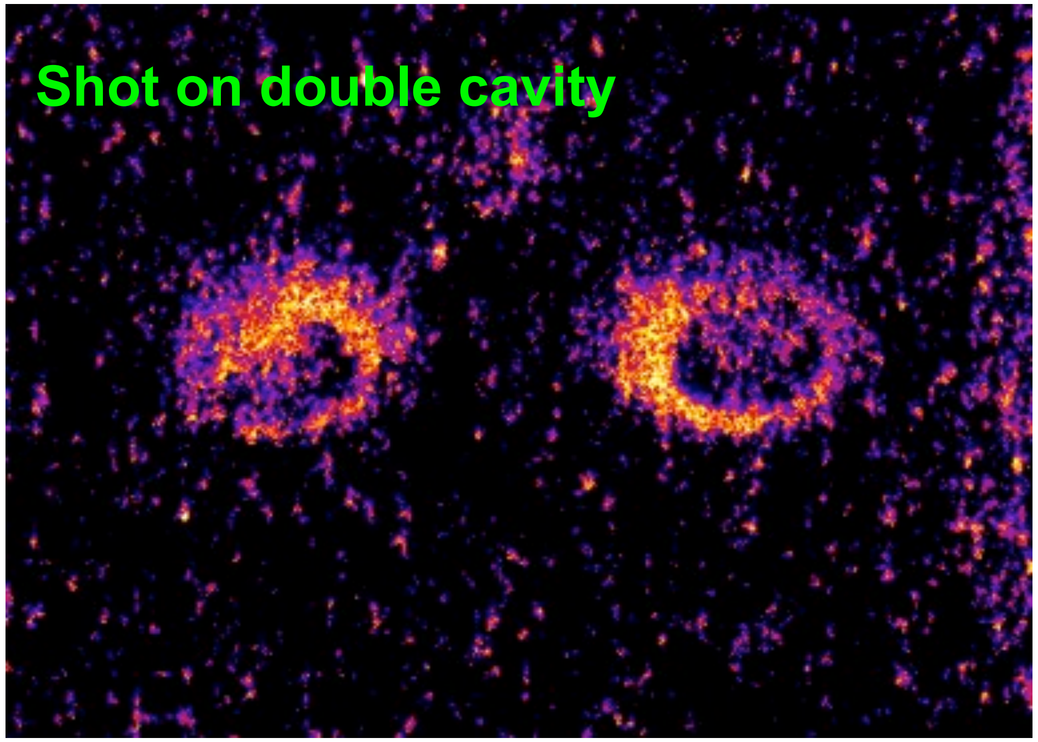

Shot on double cavity

$$\left.\frac{E_X^1}{E_X^2}\right|_{\mathrm{Au}} \simeq \frac{E_L^1}{E_L^2} \simeq \left.\frac{E_X^1}{E_X^2}\right|_{\mathrm{Cu}} \simeq 3$$

XUV opacity measurements

Heating using a double cavity

Radiation hydrodynamics calculations

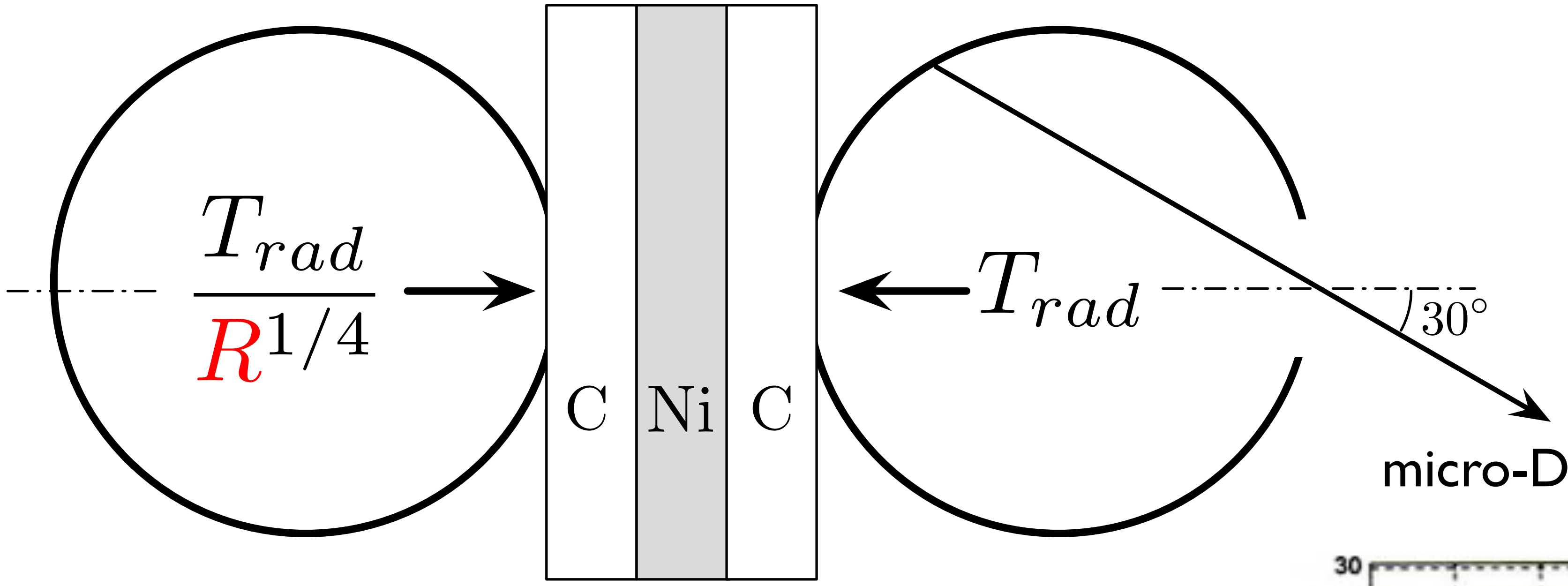

micro-DMX line of sight

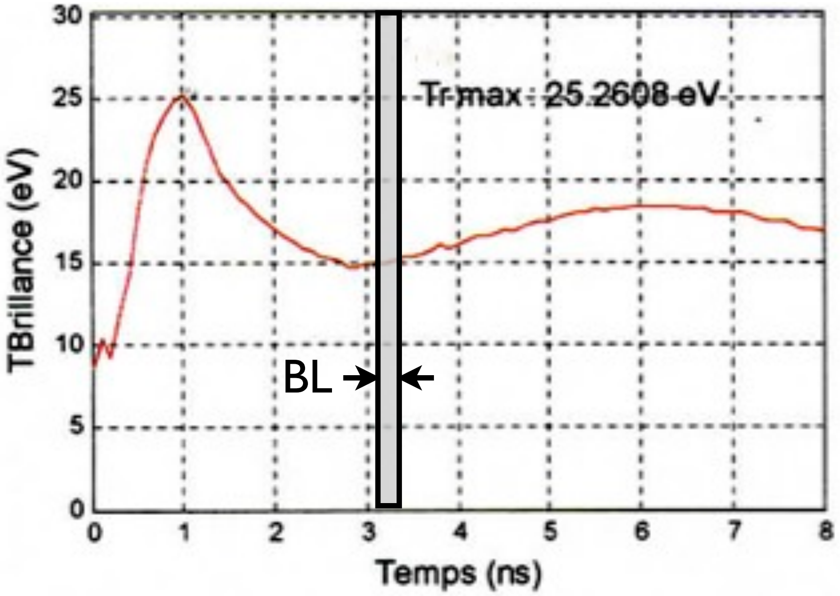

R : energy ratio right/left

Estimated radiative temperature in one cavity using micro-DMX

→ MULTI+(*) 1D simulations

Tests for *R*=1,2,3,∞

---

* *Ramis, Schmalz, Meyer-ter-Vehn, Comp. Phys. Comm. , 1988*

Busquet et al , Bull. Amer. Phys. 2008

XUV opacity measurements

Heating using a double cavity

T, ρ spatial profiles

shot 42
delay 3.2 ns

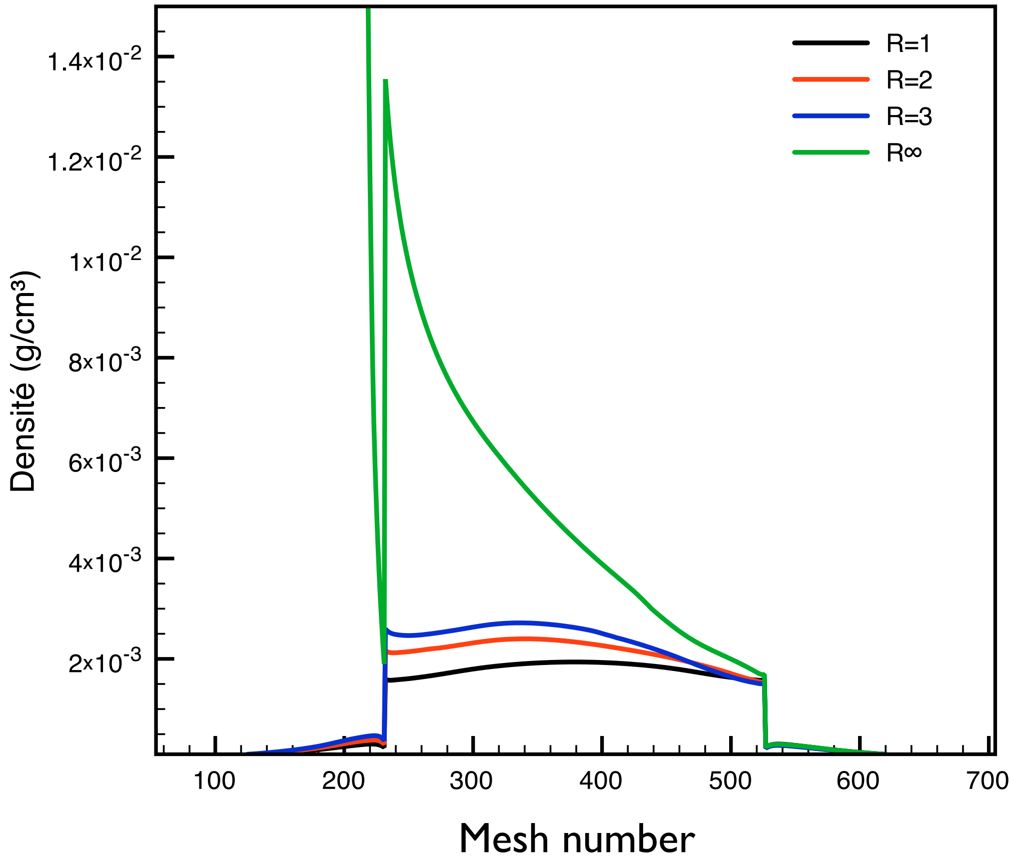

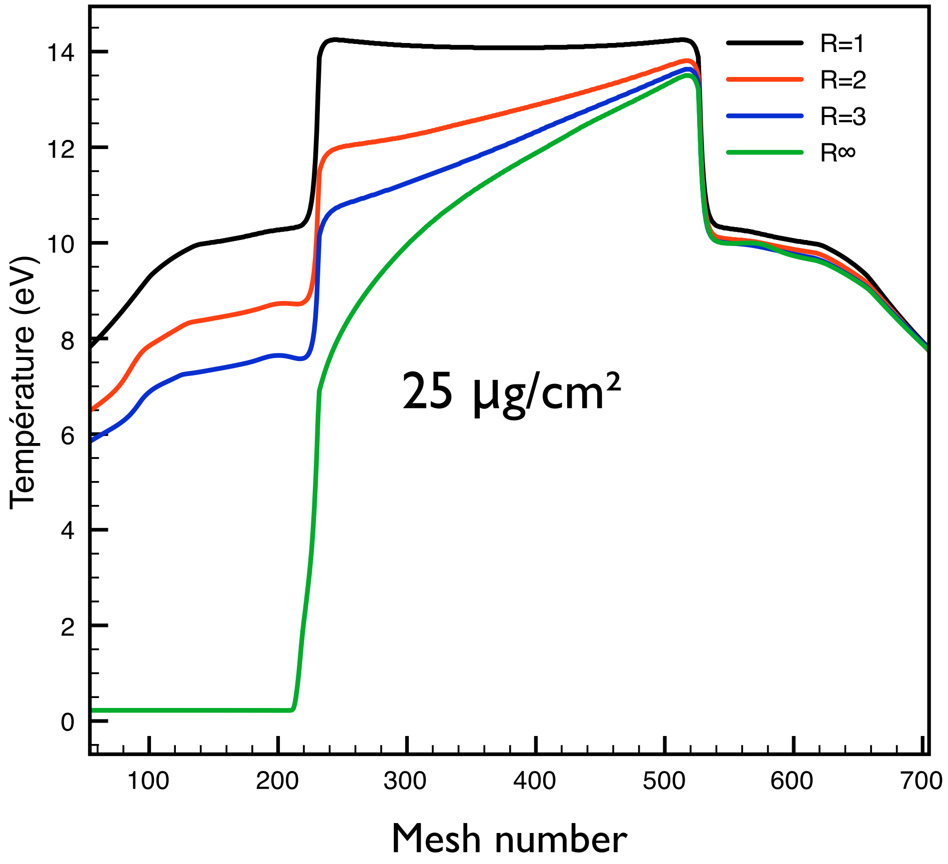

shot 49
delay 1.8 ns

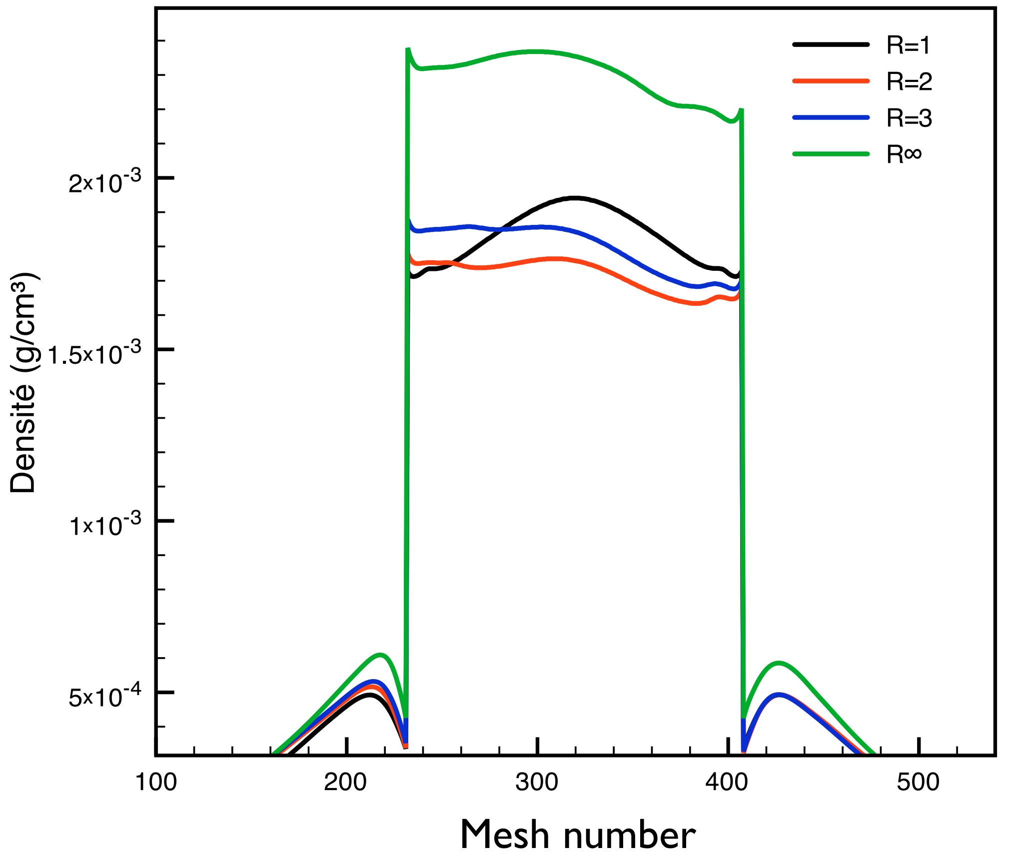

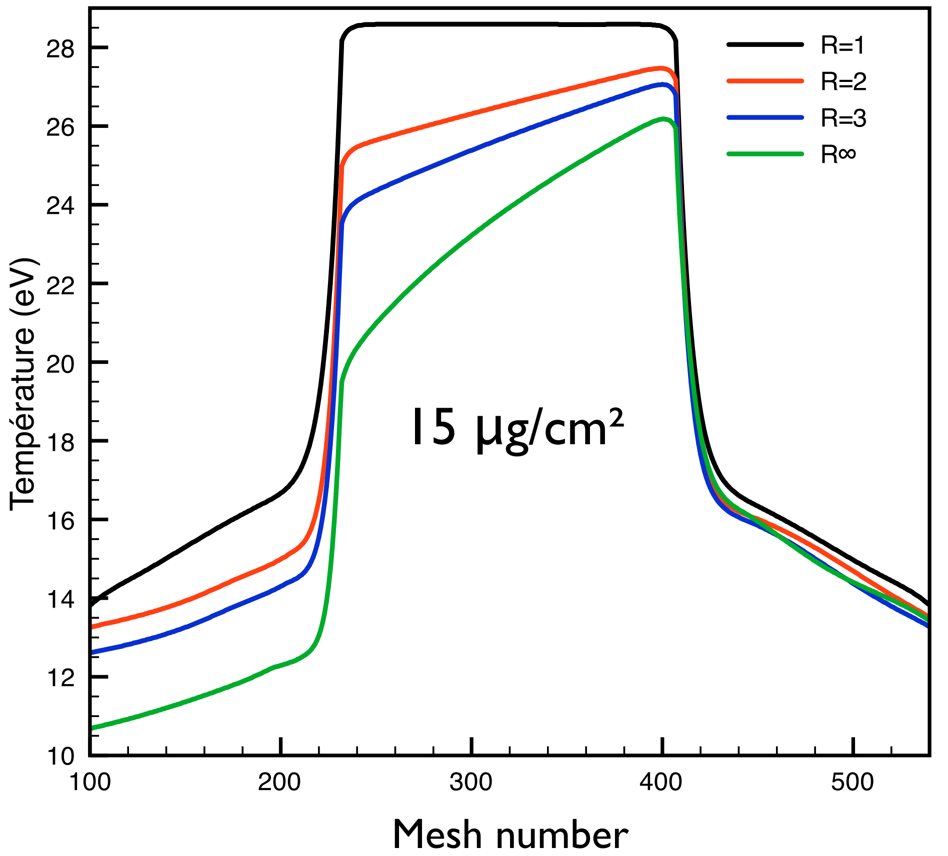

XUV opacity measurements

Nickel transmission - plasma parameters estimates

delay 3.2 ns	shot 42	$\langle\rho\rangle$ $\mathrm{mg/cm^3}$	$\Delta\rho/\langle\rho\rangle$	$\langle T\rangle$ eV	$\Delta T/\langle T\rangle$
	$R=1$	1.8 ± 0.2	17 %	14.1 ± 0.2	3 %
	$R=2$	2.1 ± 0.5	43 %	12.8 ± 1.2	18 %
	$R=3$	2.3 ± 0.6	52 %	12.1 ± 1.7	28 %
	$R\infty$	5.0 ± 6.0	240%	11.2 ± 3.3	59 %
delay 1.8 ns	shot 49 $R=1$	1.8 ± 0.1	11 %	28.6 ± 0.1	1 %
	$R=2$	1.7 ± 0.1	12 %	26.5 ± 1.2	9 %
	$R=3$	1.8 ± 0.1	11 %	25.7 ± 1.8	14 %
	$R\infty$	2.3 ± 0.6	52 %	23.7 ± 3.3	28 %

➡ Temperature gradients are reduced by a factor 2 from R∞ (one cavity only) to R=3

XUV opacity measurements

XUV spectrometer

- Toroidal mirror : concentrate light and focus on the tangential slit for spectral resolution and on the streak camera slit for spatial focus

- Reflective diffractive grating
- Use of a streak camera to discriminate in time the different emissions

➡ Spectral range 80-180 Å for ~3 Å resolution

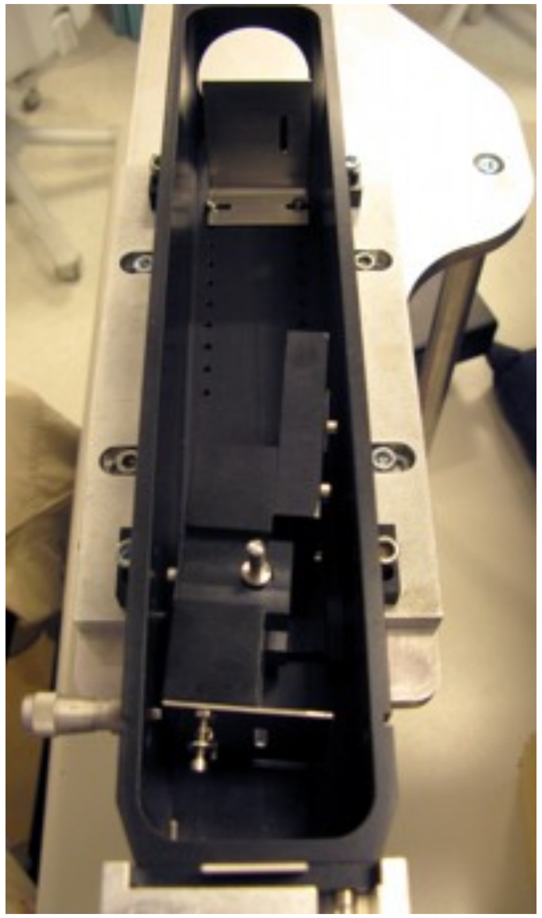

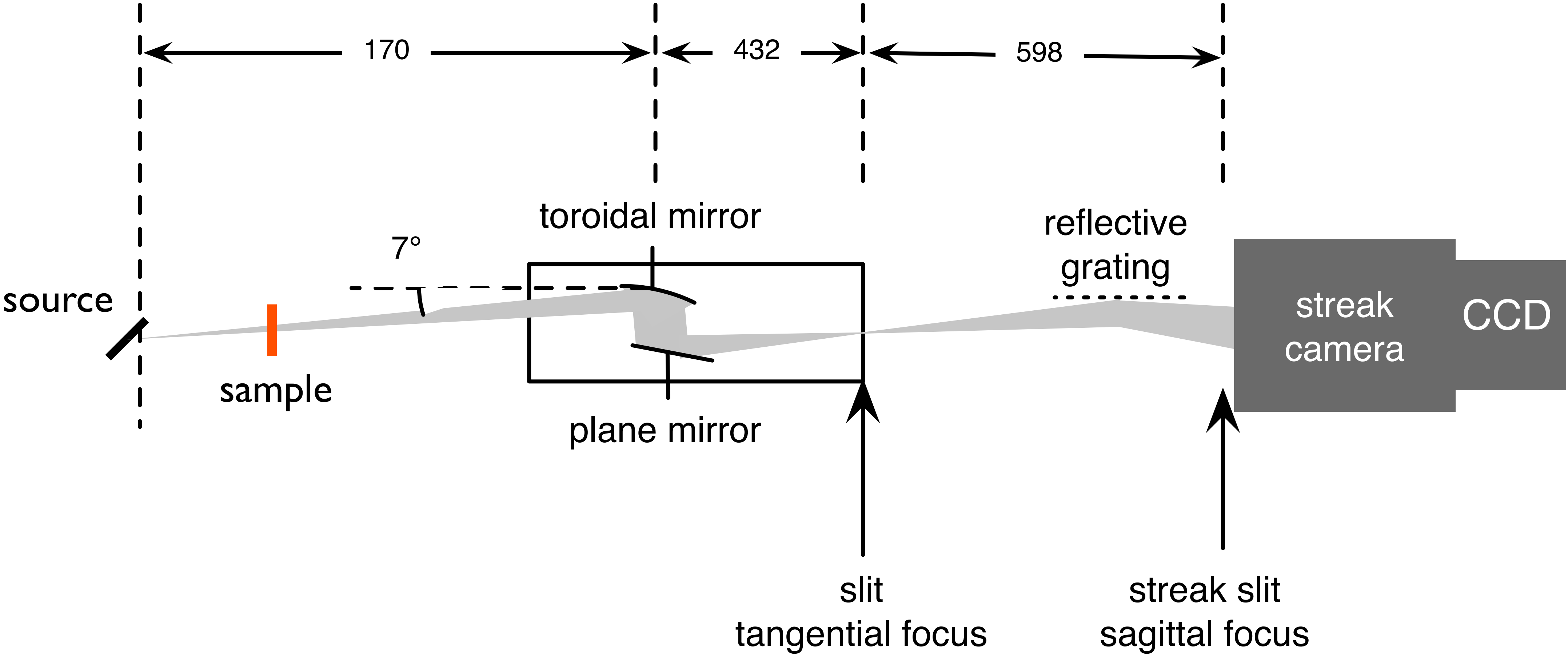

XUV spectra time evolution

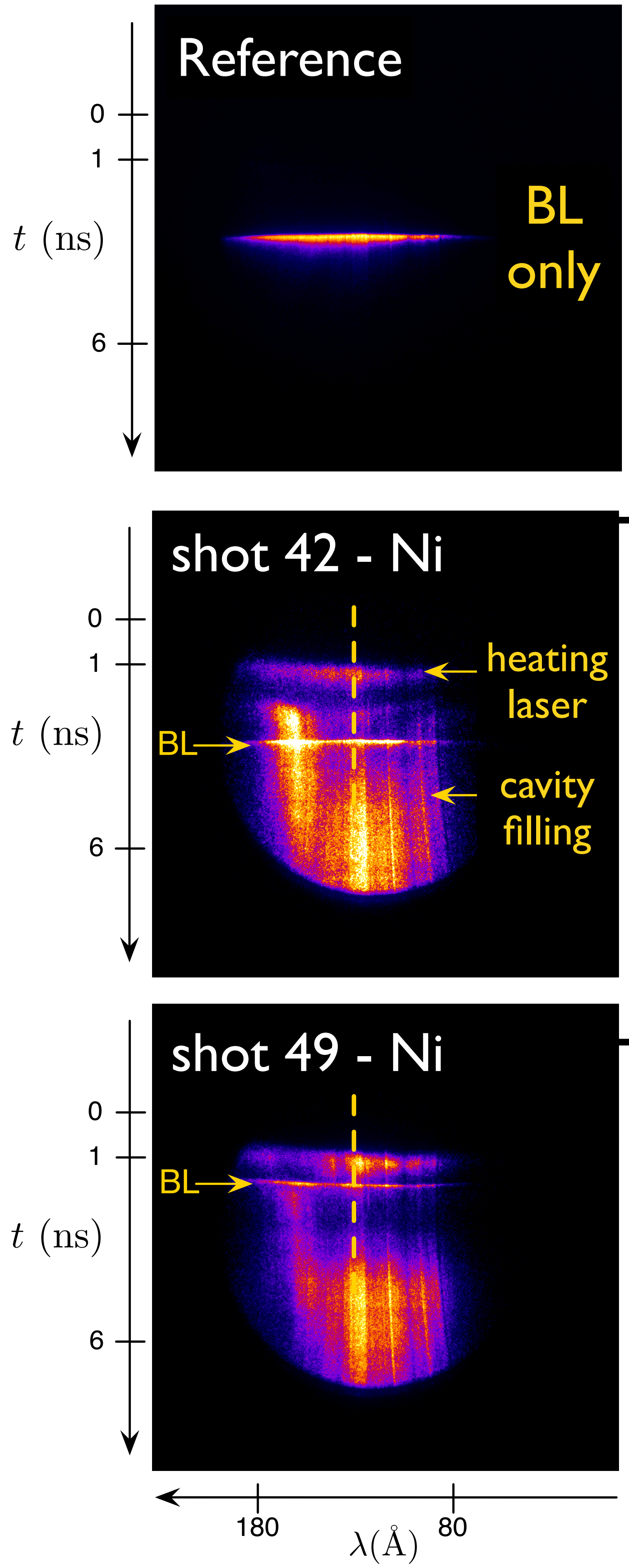

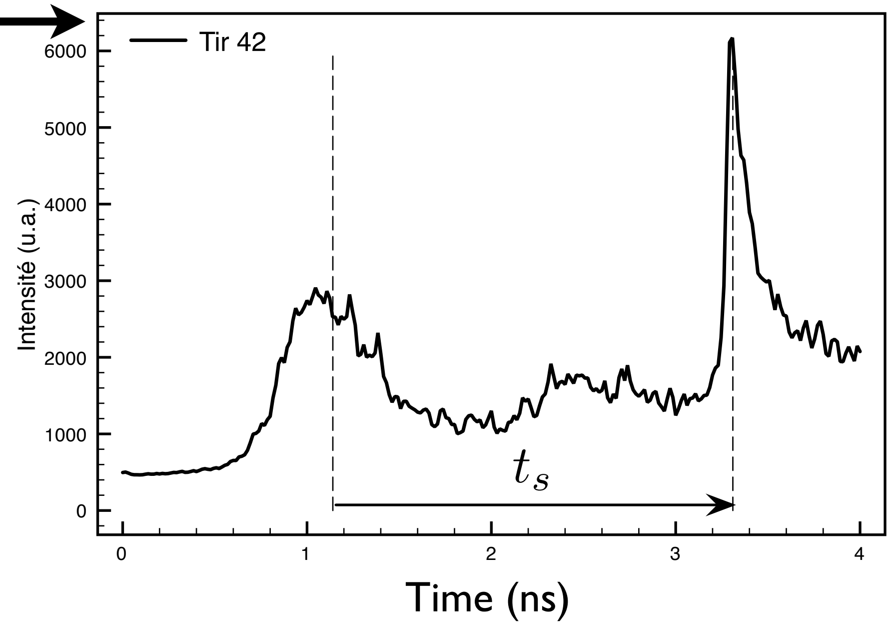

delay 3.2 ns

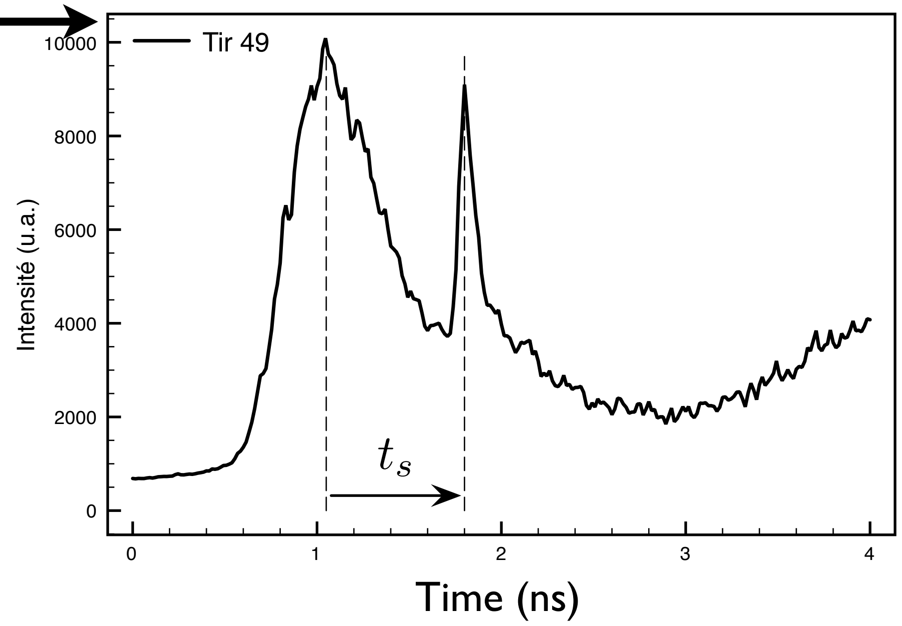

delay 1.8 ns

Spectra Transmissions

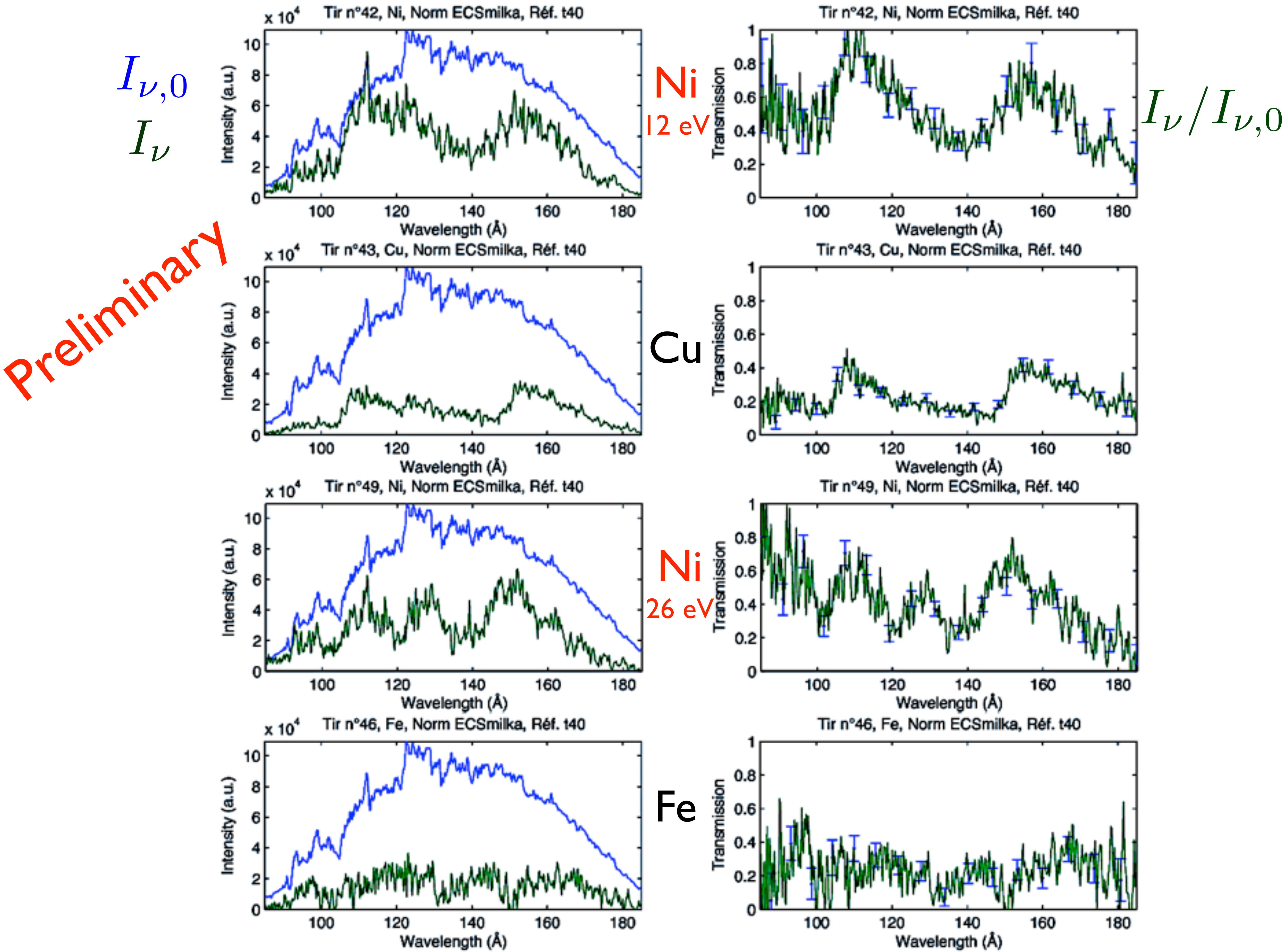

Conclusions and perspectives (1)

- X-ray absorption of Fe, Ni & Cu and of BaF_2, Gd & Sm plasmas

→ observed thermal and statistical effects on the spin orbit structure

→ check of theoretical models

- XUV absorption of Cr, Fe, Cu & Ni plasmas

→ validation of the experimental setup

→ spectra analysis in progress

- General improvements

→ on the short radiography source

→ on the heating scheme using a double cavity

Conclusions and perspectives (2)

For the future...

X-ray opacity

- use the double cavity heating to limit gradients
- perform 2D simulations of the sample evolution
- analysis of spectral data for BaF_2, Sm & Gd

XUV opacity

- measurements of the energy in each sub-beam for each shot
- broadening of the XUV spectral band
- complete simulation of the experiment

Use of both spectral domains to better constrain plasma parameters

Thank you!

Supplements

Radiography in ps regime

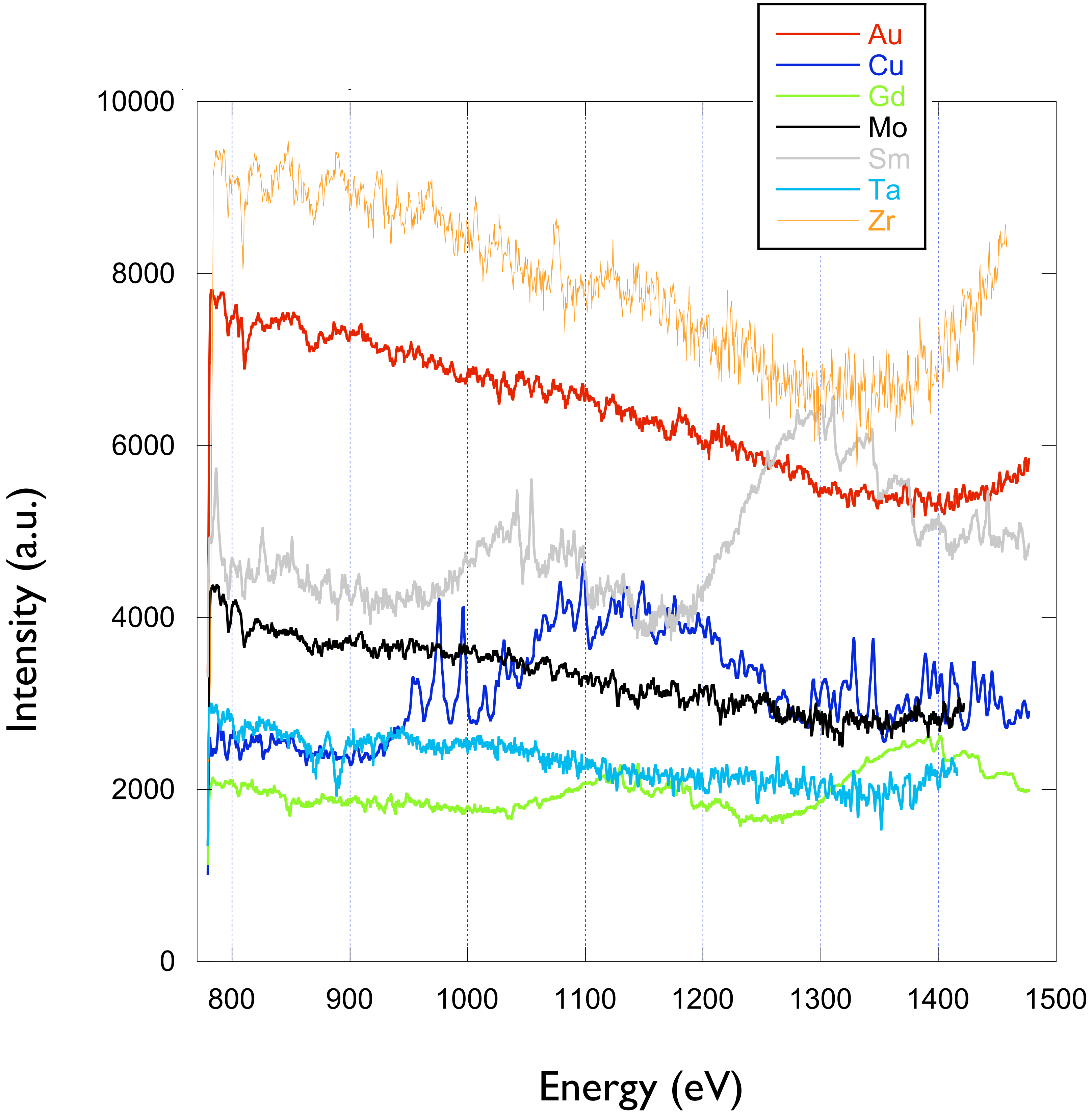

EQUINOX facility

- Plane targets
- Laser energy 180 mJ x 10 shots
- Pulses durations 80 fs, 1 ps, 10 ps

➡ Gold presents best conversion rate and most regular spectrum

β-Cephei opacities

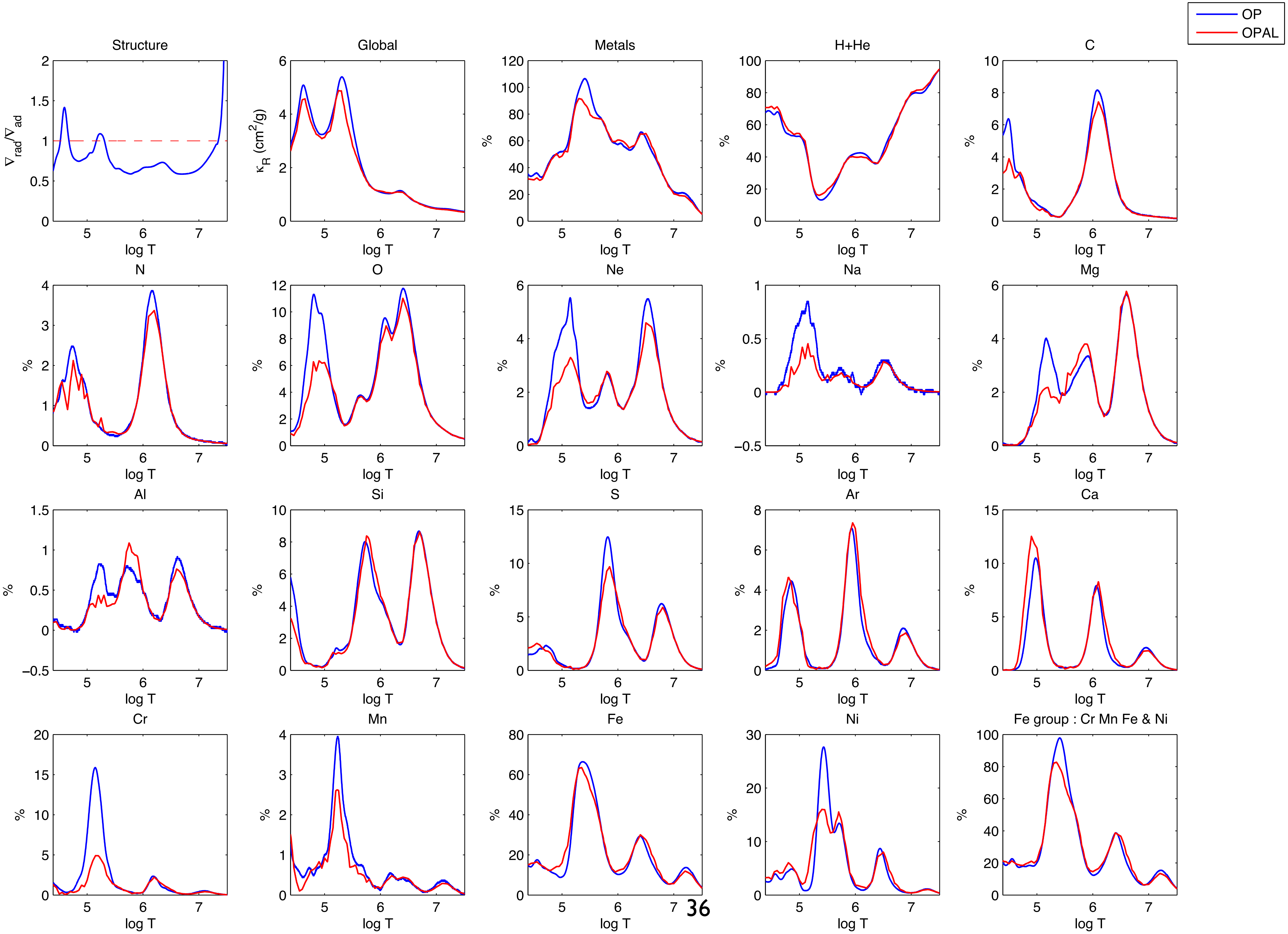

Sun opacities

Elemental contribution along the solar radius

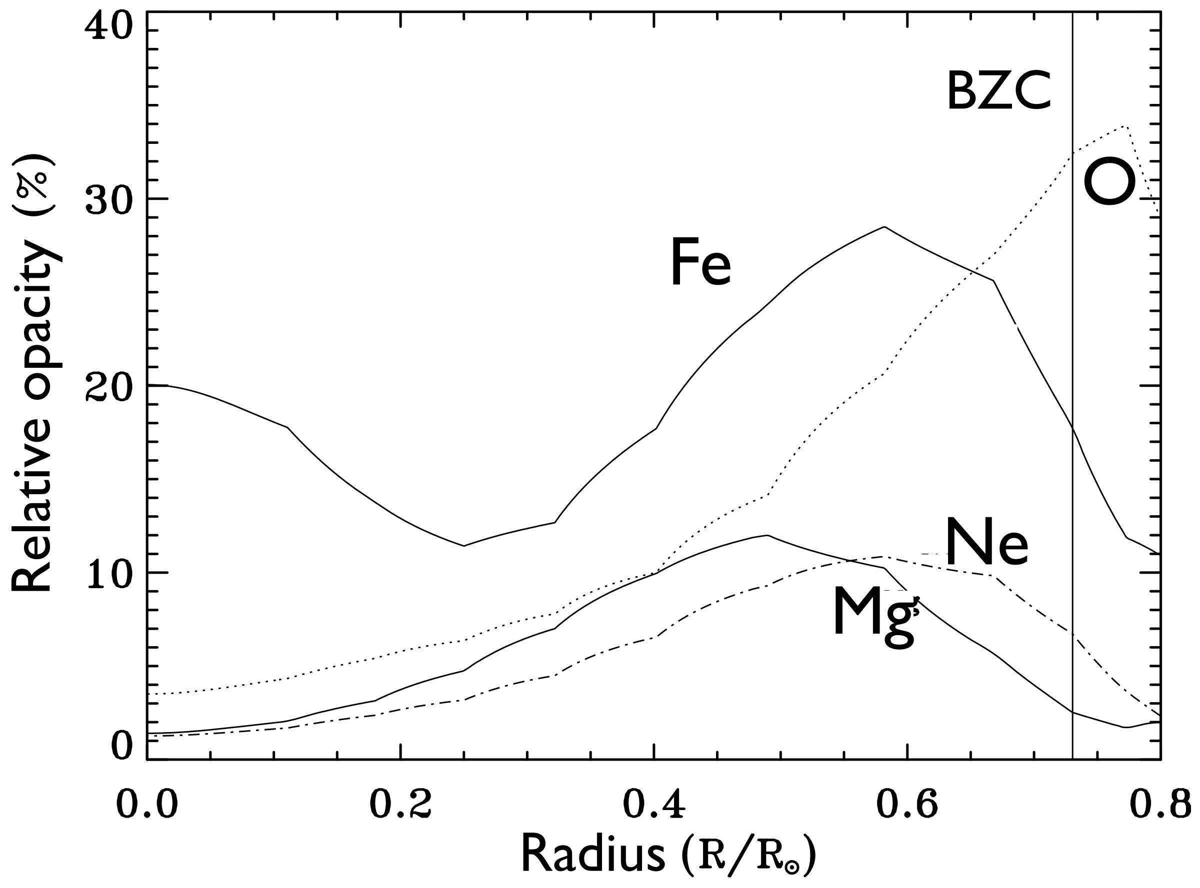

Turck-Chièze...Loisel et al., 2009

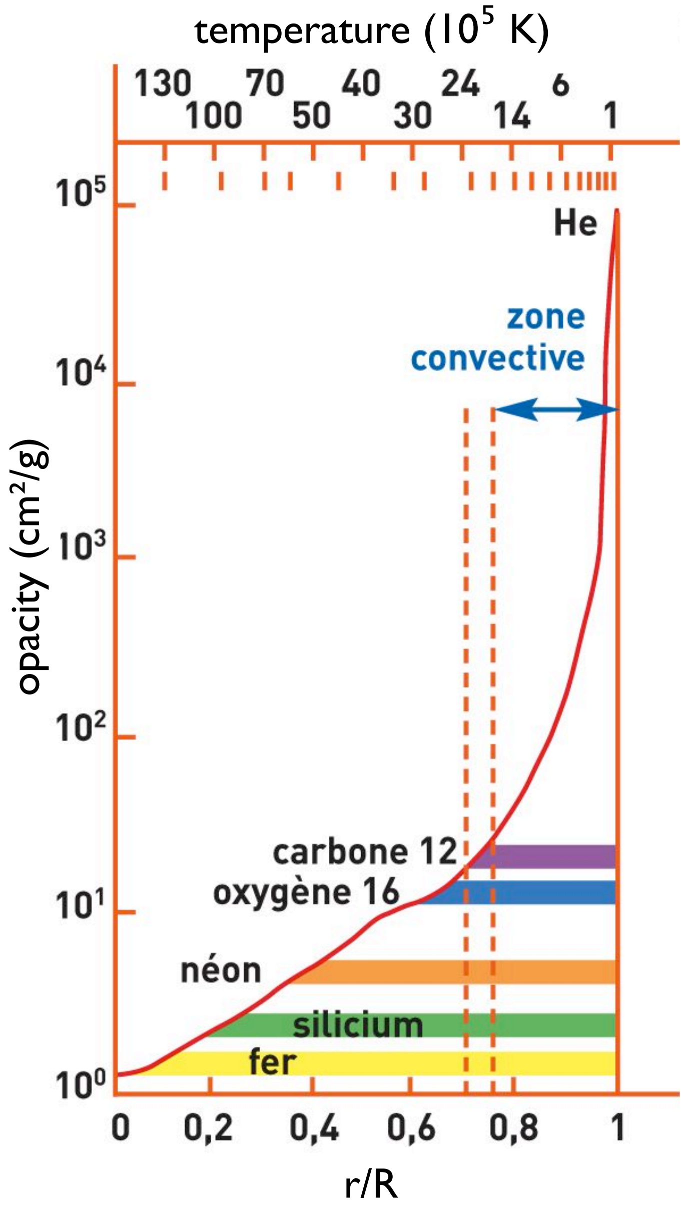

Turck-Chièze et al., 1993

Proportion Fe, O, Ne, Mg ~ 10^{-4} with respect to H